**Test Method and Fixtures for Comparing Fatigue Loading Conditions in Bones**

This report represents the work of one or more WPI undergraduate students submitted to the faculty as evidence of completion of a degree requirement. WPI routinely publishes these reports on the web without editorial or peer review.

By:
Brittany Bolster
Christina Freni
Erica Houghton
Isabelle Jaquith
Sofia Orrico

Date: 6 May 2021

Report Submitted to:
Professor Karen Troy
Professor Olufunmilayo Ayobami
Worcester Polytechnic Institute

# Table of Contents

# Table of Figures

# Table of Tables

# Acknowledgements

We would like to thank our advisors, Professor Troy and Professor Ayobami, for all their guidance throughout the project. Additionally, we would like to thank Lisa Wall, Robert Kirch, and Kyle Murdock for all their support through the project.

# Abstract

Bone stress injuries occur when the bones cannot tolerate repeated mechanical loads. This kind of injury is common in athletes, accounting for 10% of all orthopedic injuries. Early detection of bone stress injury and identification of risk factors is an essential part of injury management. This study examined how metatarsals may react under repeated mechanical loads by developing a design and test fixture to model the physiological loading conditions on avian tibia. Testing on 10 avian tibia was performed and damage accumulation up to 30,000 cycles was measured. This damage was used to identify the mechanical properties of bone under cyclic loading conditions, which can be used to inform preventative methods and treatment for bone stress injuries in humans.

# 1. Introduction

Bone stress injuries (BSIs) account for 10% of all orthopedic injuries and represent 20% of the injuries seen in sports medicine [Abbott 2020]. The number of bone stress injuries increases in running and jumping athletes, whose metatarsals are under a significant amount of stress during competition. Athletes who increase the duration, intensity, and/or frequency of physical activity without adequate periods of rest increase the risk of stress fracture during training. Bone stress injuries are driven by a multitude of factors including bone mineral density (BMD), the female athlete triad, and submaximal loading. While the incidence of bone stress injuries in the lower extremity have been recognized as one of the most prevalent, there is a gap in the research. In order to fully understand the injury and how to prevent and treat it, there needs to be a testing procedure and fixture to replicate the loading that occurs during physical activity.

Metatarsals are the long thin bones that lead to each toe in the foot. When one of these bones experiences a complete or partial break, it is considered a metatarsal injury. Metatarsal fractures account for 35% of all foot fractures and over 5% of all skeletal injuries[Petrisor 2006]. There are five metatarsal bones in the normal foot, numbered from the midline to the midaxillary line of the human body. For metatarsals one through three, the closer ends of the metatarsal bones create joints with other bones of the midfoot but they account for little movement. The fourth and fifth metatarsals with the toe bones combine to account for a significant amount of movement. The movement and location of the metatarsal bones dictate the treatment for injury [Kawaguchi 2018]. Fractures sustained by the different metatarsal bones can range from easily manageable injuries to complicated ones that require more clinical intervention. Most fractures are a result of repeated stress on the bone or foot.

When athletes engage in running and jumping activity, they increase osteoclastic activity and bone reabsorption while bone formation lags. The fatigue damage that accumulates during this time is heightened when the athlete's bone mineral density is low or they present with one or more aspects of the female athlete triad. In order to replicate fatigue damage in testing, it is necessary to understand how the damage accumulates and what effect it has on the bone. Damage is dependent on the magnitude and rate of the applied load, serving as a threshold for this phenomenon. Under repeated loading cycles, cyclic overloading occurs. In this case, remodeling is given an insufficient amount of time to repair the damage that has accumulated. The inability of a bone to withstand repetitive rounds of loading, results in structural fatigue within the affected area. After excessive loading, signs and symptoms arise as a response to localized pain and tenderness. The accumulation of damage begins as microdamage, which can be overcome by the bone through a series of self-repair and targeted remodeling. However, the damage becomes invasive as the loading repeats.

Damage accumulation that occurs in the metatarsals of running athletes can be recreated through mechanical testing on bone. Ex vivo testing on bones replicates the loading process that occurs during running or jumping activities. Evaluating the point at which injury takes place and the point at which loading has a negative impact on bone can indicate potential risk factors. Further, mechanical properties observed and calculated from fatigue testing of chicken bones will provide an analog to the biomechanical properties of human bones. To achieve this, a design fixture as well as procedure will be developed. The test fixture design models the physiological conditions of the metatarsal within the foot while the test procedure parallels the loading felt by the metatarsal during running. Using the fixture and testing method, the mechanical properties of bone under cyclic loading can be observed and results from the project can be used to inform preventative methods and treatment.

# 2. Literature Review

## *2.1 The Problem: Bone Stress Injury*

Metatarsal bone stress injury is the second most common lower limb bone stress injury, impacting around 10-20% of athletes [Pegrum, 2012]. The type of bone stress injury can vary among different athletes, genders, and ages. Tibial shaft stress fractures constitute about half of lower limb stress fractures, the next most common is metatarsal stress fractures [Pegrum, 2012]. Along with the type of bone stress injury, the severity can vary as well. The following sections will detail varieties of bone stress injuries and expand on how they can occur.

### 2.1.1 Fatigue and Damage Accumulation of Bone Stress Injuries

Fatigue stress fractures occur when normal bone is unable to repair in appropriate time as damage is occurring or stress is repeatedly placed on the bone [Pegrum, 2012]. Fatigue is defined as the reduction of material stiffness and damage accumulation is defined as the effect of testing on the subject. Fatigue can result in damage accumulation such as crack propagation. With the use of an S-N curve, stress experienced by the bone can be plotted over a number of loading cycles. The more a bone begins to fatigue, the more likely it is to experience some sort of damage accumulation. This damage can present itself on a range, from minor to extreme damage often presenting as a fracture point. Fatigue can be defined as the "propagation and initiation of cracks from cyclic loading, with a stress magnitude invariably below the materials monotonic strength" [Pegrum, 2012]. Fatigue can also be representative of the connection between fragility and fracture of bone.

### 2.1.2. Major Causes

Fatigue damage can be caused by a variety of conditions, including type of loading as well as repetition of loading. Understanding the behavior of bone in reaction to these conditions is crucial to comprehending fatigue damage as a whole. Previously conducted studies can indicate fatigue behavior and damage accumulation. In one study, a study on fatigue behavior conducted in 1981, the fatigue behavior of adult cortical bone was researched. Within this study, uniaxial fatigue tests were conducted on specimens of devitalized cortical bone to identify fatigue behavior. The results indicated that bone fatigue is gradual, and is often accompanied by an increase in hysteresis and loss of bone stiffness. This study also indicated that bone has extremely poor fatigue resistance [Carter, 1981]. Another study conducted in 2013 aimed to determine how microdamage accumulates in human vertebral cancellous bone subjected to cyclic fatigue loading. Through mechanical testing, this study was able to suggest that small amounts of microdamage in human vertebral cancellous bone can cause fatigue life to reduce. Therefore microdamage, even in small amounts, can reduce the amount of loading cycles tissue can tolerate before failure. With this knowledge of fatigue damage, the occurrence of bone stress injuries can be better understood and further analyzed.

### 2.1.3 Severity and Accumulation

The occurrence of fatigue damage and consequential bone stress injuries can be due to general overuse and the application of high loads and rates on bones and joints. When overuse occurs, fatigue damage becomes more severe which can lead to fractures in bone. Loading conditions and repetition play a major role in the occurrence of bone stress injuries, especially ones occurring from fatigue damage like stress fractures. Repetitive cyclic loading can cause chronic overloading, leading to a situation where stress reactions and fractures would be more common. Severe fractures are typically caused by twisting forces or traumatic blows, but a situation of consistent overload can lead specifically to stress fracture [Physiopedia, 2021]. Once the threshold for microdamage has been surpassed, further increases in bone strain cycles or magnitude can result in additional damage [Warden, 2014].

One common aspect of loading that is commonly studied is strike patterns, specifically of runners. Running places an individual at a heightened risk for fatigue damage and consequent stress fractures in the feet due to the repetitive loading that comes with the sport. Strike patterns and shoe conditions can have a significant impact on metatarsal loading during running. [Sun, 2018]. Runners also may have to adapt their strike patterns due to shoe durability and ground stiffness, which can affect fatigue damage. However, the influence of strike patterns is more significant than shoe conditions when fatigue damage is being considered. There are other variables to consider when analyzing why fatigue damage occurs, such as external factors like shoe durability or ground stiffness. However, in one 2018 study on the landing strike patterns of male runners, rearfoot versus forefoot strike patterns and the influence of footwear was investigated. It was concluded that the influence of strike patterns on running was more significant than that of shoe conditions [Sun, 2018]. Another important consideration is the difference between forefoot and rearfoot strike patterns. This difference, although seemingly small, could have major implications on the occurrence of fatigue damage and consequent bone stress injuries. Runners with rearfoot strike patterns have shown reduced maximum loading rates while runners with forefoot strike patterns have shown to increase maximum push-off force

[Sun, 2018]. Plantar loads can vary. A 2019 study comparing plantar loads among male runners with different strike patterns focused on the loading variability between rearfoot and forefoot strikes. It was found that force and pressure parameters have proven to be higher in the rearfoot and midfoot regions during rearfoot strikes, and relatively greater in the forefoot region during forefoot strikes. Similarly, the contact area, max force, and force-time integrals are higher during rearfoot strikes. On the other hand, forefoot strike patterns seemed to have a specific correlation to metatarsal stress fractures [Wei, 2019]. It can be determined that both rearfoot and forefoot strike patterns Conclusively, it was determined that either strike pattern, under intense repetitive loading like in running, can place an individual at risk for fatigue damage. This conclusion emphasizes that even though repetitive loading behavior is perceived to lead to bone stress injury, limited research has been done to actually expand on the topic.

**2.1.4 Loading Condition Changes**

Fatigue and damage accumulation can also occur as a result of an increase in weight or number of cycles during loading. Another cause for fatigue accumulation in regards to loading conditions is a drastic increase in cycles or weights. Bone stress injuries, especially stress fractures, can be gradual. Before fatigue damage gets to a point of alteration, the healthy bone is able to conduct a normal remodeling process that does not result in a fracture. However, this process can be escalated with an introduction to higher loads as well as an increase in loading cycles. A study conducted in 2002 aimed to understand metatarsal stress fracture etiology can provide a fundamental description of loading patterns of the metatarsals during loading [Arndt, 2002]. This study also investigated the idea that metatarsal strain increases with fatigue and external carrying loads. by exposing their subjects to a 20kg load increase in the form of a backpack. This study made the important conclusion that metatarsal deformation and strain alterations are contributing factors in the progression of stress fractures. In the case of this study, the change in load was relevant in the progression of metatarsal stress fractures. As the loading weight increased, the bones were unable to adapt quick enough to remain strong. This led to a significant increase in fatigue accumulation, eventually leading to bone stress injury. Along with this, sharp change in loading cycles and or loading patterns can result in microdamage accumulation as well [Warden, 2014].

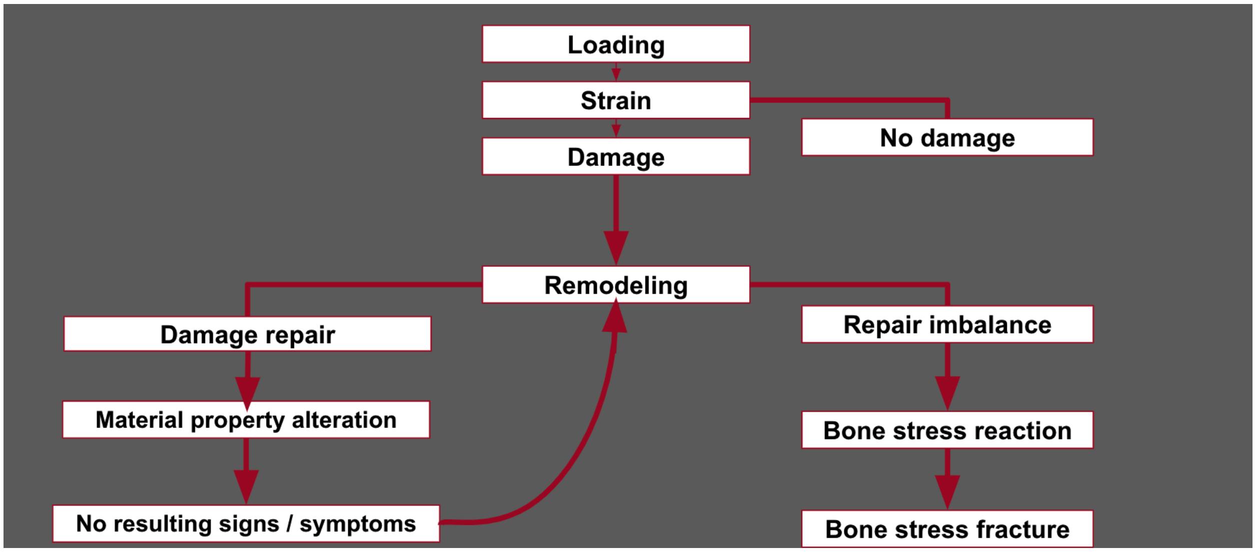


*Figure 1: Flow chart depicting the process of bone damage accumulation.* [Adapted from Warden, 2014]

## *2.2 Who Bone Stress Injuries Affect Most and Why*

### 2.2.1 Women

There is a high risk of stress fractures due to the female athlete triad which can be described by low energy availability due to disordered eating, menstrual dysfunction, and low bone mineral density. This set of risk factors can affect bone metabolism. In some studies, the incidence of stress fractures in female athletes has been up to thirteen percent. The risk of stress fracture among females who present any aspect of the triad is dependent on how many aspects they present with. The risk to a female with one aspect of the triad is between fifteen and twenty percent, while the risk to a female that presents with multiple aspects of the triad can be up to fifty percent [Abbott, 2020].

In a study conducted by Kathryn Ackerman, fracture prevalence was compared among three groups: oligo-amenorrheic athletes, eumenorrheic athletes, and non-athletes. Oligomenorrhea is defined as the absence of menses for at least three months within a period where cycle length is greater than six weeks for at least six months before the study. Oligo-amenorrheic athletes could also include athletes over the age of fifteen with the absence of menarche. The results of the study revealed that there is a significantly higher incidence of stress fractures in oligo-amenorrheic athletes due to a lower bone mineral bone density in comparison to eumenorrheic athletes and non-athletes [Ackerman, 2015].

### 2.2.2 Athletes

Bone stress injuries are prevalent increasingly common among athletes. Stress fractures of the foot are most common in running and jumping athletes, with an increased risk for athletes who increase duration/intensity/frequency of physical activity without adequate periods of rest. While the incidence of stress fractures in the general athletic population is less than one percent, the percentage increases to fifteen percent in runners alone. Two of the three sports where stress fractures are most commonly seen are women's cross country and women's outdoor track. The third sport is women's gymnastics. When comparing women to men, stress fracture rates in female athletes were over twice as high as the rates for male athletes. Out of 100,000 athlete exposures, 9.13 women had experienced a stress fracture and only 4.44 men had experienced stress fractures [Rizzone, 2017]. The most common stress fracture locations include the metatarsals, tibia, and the lower back/lumbar spine/pelvis. Metatarsal fractures are statistically most common, claiming around 37.9% of all fractures per 1000,000 athletes [Rizzone, 2017].

## *2.3 Properties of Bone*

### 2.3.1 Bone cells

Bone cells affect the onset of injury and the rate of healing. Bones are made up of cells called osteocytes, osteoclasts, and osteoblasts.Osteocytes are derived from osteoblasts, and represent their mature/inactive form. They lay within the bone rather than the surface, occupying the lacuna. The main role of osteocytes is to respond to mechanical strain and send signals of bone formation or bone resorption to the bone surface. These mechanisms modify and regulate local and systemic homeostasis. Osteoclasts break down existing bone, while osteoblasts help to form new born and support the growth of existing bone.

### 2.3.2 Bone Composition

Bone composition has a direct effect on the mechanical properties of the bone. Cortical bone is dense and surrounds the cancellous bone, which is porous. The mechanical behavior of bone includes viscoelasticity and fracture. However, the mechanical behavior of cortical and cancellous bone at the macrostructural level may vary from one bone to another as well as within different regions of the same bone. Viscoelasticity is a time-dependent reduction in stress that occurs when bone is under constant strain. Fracture can occur during different loading conditions, Both tension and compression occur during axial loading. The main difference between a compressive fracture and a tensile fracture is that the deformation curve of a compression specimen contains a short yield region. The load in a compressive fracture drops slightly and then continues at the same level until the specimen breaks [Currey, 2006]. Fracture can also occur under bending circumstances. Finally, fatigue fracture results from stresses imposed by the muscular system during locomotion.

#### 2.3.3 Bone Remodeling

Loading conditions cause the bone to be subject to constant stress. As a result of repetitive loading, bone remodeling occurs. Bone remodeling serves to replace fatigue-damaged bone while creating temporary porosity. In response to mechanical loading, bone forms on the periosteal surface of long bones to improve fatigue resistance. The degree to which bone remodeling occurs is dependent on fatigue life, which can be defined as the number of loading cycles a material can sustain before failure. Multi-axial loading can lead to abnormal loading patterns and shear stresses, ultimately reducing the fatigue life [Hughes, 2017].

The effect of bone remodeling on stress fractures varies from bone to bone. In some cases, bone remodeling can promote stress fracture development by introducing an acute increase in porosity. In other cases, bone remodeling can prevent stress fracture development by replacing fatigue damaged bone. After repetitive loading, an initial period immediately follows during which the bone acquires microdamage. Microdamage decreases the elastic modulus of the bone, leading to a cumulative bone stress injury.

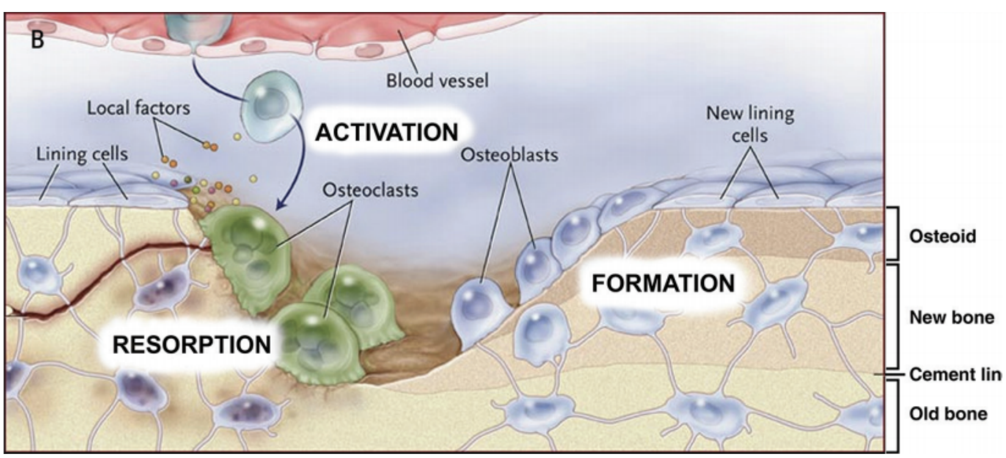


*Figure 2: Bone microdamage and target remodeling.* [Warden, 2014]

### *2.4 Why is This Important*

The presence of bone stress injuries is relevant throughout undeniably relevant, especially in the lives of athletes. The impact of stress accumulated bone stress injuries, like metatarsal stress fractures runs deep for all who participate in athletics, but most relevantly for runners. The cyclic loading incorporated in the sport of running puts those individuals at higher risk for developing stress fractures and bone stress injuries. There are a multitude of factors that contribute to stress accumulation in bone, all of which play a role in the development of stress fractures. However, although lower extremity injuries are commonly studied, there is a lack of understanding in how loading conditions and fatigue damage are related. This lack of research prohibits advancements in preventative medicine in relation to metatarsal stress fractures.

# 3. Project Strategy

This chapter outlines the intentions of the project. There are many steps involved in creating the direction of our design. Our approach began with the initial client statement provided by Professor Troy. Within this client statement, we were able to understand the goals for our project. Following, the clarity of our goals allowed us to define our requirements. These requirements were broken into objectives as well as constraints. The rankings were compared and prioritized. Ultimately, we developed a revised problem and client statement as well as three main aims to frame our project outlook.

## *3.1 Initial Client Statement*

The initial client statement was provided to us by Dr. Karen Troy, our project advisor.
Higher cyclic strains are associated with more rapid damage accumulation and BSI risk. Cadaveric studies demonstrate that activation of the muscles supporting the arch can reduce metatarsal surface strain, and epidemiologic studies link foot weakness to increased risk of metatarsal BSI. The suggests that activation of the foot muscles, which is modifiable, may potentially protect the metatarsals from BSI by altering the magnitude and direction of applied forces.

- Design fixturing and test protocols to compare the effect of bending vs axial loading on whole bone fatigue failure / damage accumulation.
- Use imaging and engineering methods to calculate and then assign stress and strain for each specimen.

- Perform fatigue testing on avian bone specimens loaded in different directions (axial vs. axial+bending).

## *3.2 Technical Design Requirements*

After the client statement was established, we decided that there are two aspects of the design portion of our project, including the Test Method and the Test Fixture. From there, the following design objectives and constraints were constructed.

### 3.2.1 Design Objectives of Test Methods

- Adaptable: The test method must be applicable for different types of tests that may be needed in the future. Adaptability will allow the team to easily shift test methods if it becomes necessary and will allow the same for future teams.
- Bone Sizing: The test methods will utilize a specimen with a similar cortical diameter to a human metatarsal. If a similar cortical diameter is not conceivable, the methods should utilize bone specimens with similar composition and shape as the metatarsal. Maintaining this standard will allow the results to be compared to human specimens.
- Physiologically Relevant: The test method must use values that are physiologically relevant to the conditions it aims to address. In this case, the team is trying to simulate loading patterns involved in running. The test methods should allow for simulation of those loads.
- Show Fatigue Accumulation: The test method should test the specimens in such a way that fatigue can accumulate properly for analysis. The test method should allow the specimen to fatigue gradually so a progressional change can be visualized and understood.
- Safety Features: The test method should account for the reassurance of all safety precautions before the beginning of the test. The methods should also incorporate the use of safety stops and maintain safety through the end of the test.
- User-Friendly: The testing method should be repeatable in nature and easily understood by first-time users. The method should include the assurance that the specimens are solidly in place, minimizing the risk of slippage or general user error.

A Pairwise comparison was composed by the team to rank the test method objectives as compared to one another. The pairwise comparison for the test method can be seen below in

Table 1. Then, using the pairwise comparison, the team determined the test method objectives most relevant to the project. Table 2 shows the order of importance based on the analysis of the comparison.

*Table 1: Pairwise comparison chart for the test method objectives.*

| | **Adaptable** | **Bone Sizing** | **Physiologically Relevant** | **Show Fatigue Accumulation** | **Safety Features** | **User-Friendly** | **Totals** |
|---|---|---|---|---|---|---|---|
| Adaptable | -- | 0 | 0 | 0 | 0 | 0 | 0 |
| Bone Sizing | 1 | -- | 1 | 1 | 0 | 1 | 4 |
| Physiologically Relevant | 1 | 0 | -- | 1 | 0 | 1 | 3 |
| Show Fatigue Accumulation | 1 | 0 | 0 | -- | 0 | 1 | 2 |
| Safety Features | 1 | 1 | 1 | 1 | -- | 1 | 5 |
| User-Friendly | 1 | 0 | 0 | 0 | 0 | -- | 1 |

*Table 2: Results from the Pairwise comparison analysis.*

| **Final Rankings** |
|---|
| Safety Features |
| Bone Sizing |
| Physiologically Relevant |
| Show Fatigue Accumulation |
| User Friendly |
| Adaptable |

### 3.2.2 Design Objectives of Test Fixture

- <u>Precision/Accuracy:</u> The testing fixture holds the specimen at a standard and repeatable location to allow for correct crack propagation and formation. The fixture should minimize any slippage between trials.
- <u>Stress/Strain Relief (No Preload):</u> The testing fixture should allow for stress/strain relief meaning that there is no preload applied to the specimens in between each test. Each test should be independent of the previous one to show the relevance of consistent and stable force application.

- Sizing Constraints for the Machine: The testing fixture should not exceed the size limitations presented by the machine being used. The fixture should assimilate into the machine and not negatively impact the functionality of the machine.
- Safety: The testing fixture should not inhibit the safety features of the testing machine. The fixture should also not put those utilizing its capabilities at any sort of risk.
- Durable: We aim to perform around 500,000 cycles per specimen on multiple specimens. The testing fixture must be able to withstand the testing.
- Non-corrosive: The specimens will need to remain hydrated. Therefore, the fixture must be able to be exposed to the hydration fluid and not have any chemical response to them.
- Axial Bending Accommodation: The testing fixture should accommodate for cyclic axial loading as well as cyclic bending test procedures. In order to understand different properties of the specimens, both cyclic axial and bending tests should be performed and the fixture should be able to assist in both procedures.

Similar to the test method, a Pairwise comparison was composed by the team to rank the fixture objectives as compared to one another. The pairwise comparison can be seen below in Table 3. Then, using the pairwise comparison, it was determined which fixture design objectives are most important to the project. Table 4 shows the order of importance based on the analysis of the comparison.

*Table 3: Pairwise comparison chart for the testing fixture objectives*

| | Precision/ Accuracy | Stress/Strain Relief (No Preload) | Sizing Constraints | Safety | Durable/ Reusable | Non-corrosive | Axial Bending Accomodation | Totals |
|---|---|---|---|---|---|---|---|---|
| Precision/Accuracy | -- | 0 | 0 | 0 | 0 | 0 | 1 | 1 |
| Stress/Strain Relief (No Preload) | 1 | -- | 0 | 0 | 1 | 0 | 1 | 3 |
| Sizing Constraints for the Machine | 1 | 1 | -- | 0 | 1 | 1 | 1 | 5 |
| Safety | 1 | 1 | 1 | -- | 1 | 1 | 1 | 6 |
| Durable | 1 | 0 | 0 | 0 | -- | 0 | 1 | 2 |
| Non-corrosive | 1 | 1 | 0 | 0 | 1 | -- | 1 | 4 |
| Axial Bending Accommodation | 0 | 0 | 0 | 0 | 0 | 0 | -- | 0 |

*Table 4 : Results from the Pairwise comparison analysis*

| Final Rankings |
|---|
| Safety |
| Sizing Constraints |
| Non-Corrosive |
| Stress/Strain Relief |
| Durable |
| Precision Accuracy |
| Axial Bending Accommodation |

#### 3.2.3 Constraints

- Project Duration: The project should be completed throughout the academic year, spanning from September-April.
- Cost: The overall budget for this project is $250 per each group member, totaling $1,250. However, the cost of the fixture designed should not exceed $500.
- Hydration of the Specimen: The bone must be hydrated in saline solution throughout the duration of the test.
- Loading Magnitude and Direction: In order to inform prevention and treatment of fatigue damage in metatarsals, the testing protocol and fixtures must recreate/model the forces on the metatarsal physiologically relevant to running.
- Cyclic Loading: Test can call for up to 500,000 loading cycles per specimen.

### *3.3 Standards for Design Requirements*

Because the project will not involve voluntary human subject testing or be used for anything outside of the scope of the project, there are no standards that the design itself must adhere to. However, the testing portion of our project as well as the MQP as a whole must adhere to ABET standards as set forth by the Biomedical Engineering Department at WPI. The testing must be completed as set by the safety and testing protocols for software and mechanical testing included in Chapter 5.

### *3.4 Revised Client Statement*

The client statement was given by the project advisor, Dr. Karen Troy, and therefore, did not need revisions. However, after reading and understanding the client statement provided, the group formulated a statement to help guide our project over the course of the year. It reads as follows: Bone stress injuries, most commonly seen in running and jumping athletes, are associated with loading conditions during activity. Although lower extremity injuries are commonly studied, there is a lack of understanding in how loading conditions and fatigue damage are related. For this reason, there is a need to study the accumulation of fatigue damage within the metatarsals to inform prevention and treatment methods.

### *3.5 Project Approach*

Aim 1: Determine physiologically relevant values for bone and use these values to determine any additional information necessary for mechanical fatigue testing. From research on metatarsal BSI's, metatarsal dimensions, and known methods for mechanical fatigue, an initial design method based upon the important fatigue properties of bone: bone diameter, volume, length cross sectional area, and the average running microstrains will be established by the team. Bluehill software will be used to create a fatigue testing program for the Instron Electropuls 3000, based on the methods developed by the team.

Aim 2: Create a test fixturing design to secure the bone during testing. From research, fatigue test fixtures for axial loading and bending will be developed by the team, based on research and fixtures already developed to fit into the machine for testing. With the dimensions of the Instron Electropuls 3000 interfaces known, we plan to design a computer aided design (CAD) software that can be used to further develop plans for designing the testing fixture. From the 3D model, we will further advance our design through drawings with dimensions and tolerances that can be created and then used to fabricate the preliminary fixture in Washburn Shops. Compatibility with the Instron and effective use for the test method will be evaluated in the preliminary testing, with modifications and documentation by team members  being made before testing begins.

Aim 3: Utilize the test fixture and test method to conduct fatigue testing on avian specimens to assess damage accumulation. The team goals for Goals of the fatigue tests include: evaluate the damage accumulation by loss of bone stiffness and analyze bone damage outcomes in axial loading, bending, and a combination of the two. Once we analyze the data this data is analyzed, conclusions can be drawn regarding the relevance to human metatarsals.

# 4. Design Process

## *4.1 Needs Analysis*

Needs analysis begins with a review of the current test process or approach to testing. After evaluation, required design features can be determined. In preparation for experimental design, there are certain specifications that need to be fulfilled. Design specifications can be separated into two categories; specifications for the test method and specifications for the test fixture.

### 4.1.1 Test Method

The test method shall account for the check of all safety features before the test even begins. It shall also call for a specific type of specimen with a similar cortical diameter to a human metatarsal. In the event that the method does not call for diameter similarity, it should be able to account for a bone specimen that has similar composition and shape to the metatarsal bone. It is necessary for the test method to use values that are physiologically relevant to running loads so that the test can produce realistic results. Results will also benefit from the test method;s ability to test specimen failure. The test method should also be able to show the fatigue progression in the specimen during testing. In order to account for the user, the test method should notify the user if there is any incidence of slippage during the test. In the event that adjustments need to be made for future testing, the test method should be adaptable.

### 4.1.2 Test Fixture

The test fixture shall not inhibit the safety features that have been set by the testing machine. In order for the fixture to work with the testing machine, the fixture must align with the specifications set by the machine. Therefore, the fixture should align with the diameter, length and width of the testing machine. Another important aspect to consider when designing the test fixture is that it must account for the hydration of the specimen. During testing, the bone needs to be hydrated. The fixture should account for the material selection and not deteriorate during testing. Testing performance may be impacted by the stress and strain that the specimen experiences, therefore the testing fixture should allow for stress and strain relief during testing. During testing, multiple tests will be run to allow for the collection of data. Due to the fact that testing will be repetitive, the testing fixture must be able to withstand multiple tests in a row. The testing fixture shall hold the specimen at the proper locations during testing. The precision and accuracy built into the testing fixture will allow for correct crack propagation and formation. In addition, the testing fixture must accommodate for cyclic axial loading as well as axial bending. Finally, the testing fixture is going to be moved throughout the test process. Therefore, it should be a portable fixture that can be moved back and forth between people and different lab locations.

## *4.2 Alternative Designs*

At the beginning of fixture design development, it was necessary to evaluate the available fixtures. By evaluating the fixtures currently available, we could define aspects to be replicated in our own test fixture. Available fixtures provided a basis for what needed to be changed to account for the goals to be achieved during our experiment. After needs analysis, we were able to develop various fixture designs to be used during testing.

### 4.2.1 Staircase Design

Figure 3 below shows the computer-aided staircase design. The idea behind this design is that it will provide relief to the bone being tested, and diminish the constraint felt by the bone during testing. The disadvantages to this design include that it may increase the chance of axial displacement and slipping. After consideration, it was determined that the staircase design may only be applicable for axial compression, not axial bending.

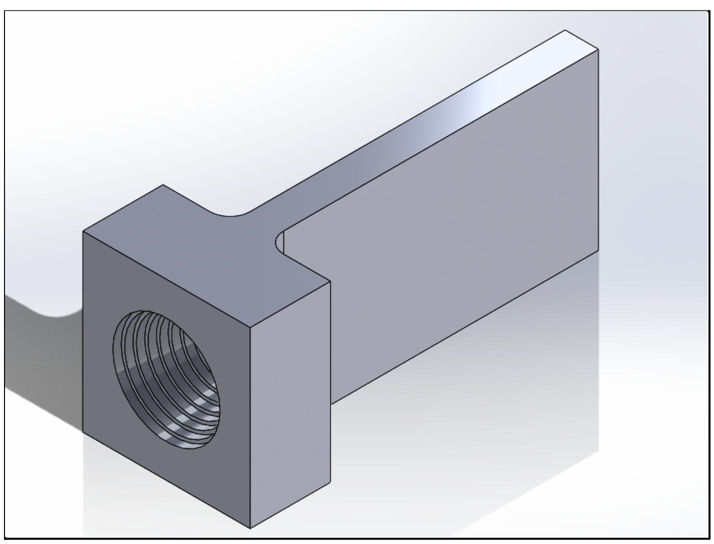

*Figure 3: Staircase Design*

### 4.2.2 Resin-Incorporated Design

Figure 4 below shows the resin-incorporated design. The advantages to this design fulfill many of the testing requirements. This design can be used for both axial compression and bringing. The incorporation of resin decreases the chance of axial shifting and slipping, which could inhibit the ability to produce accurate results. The resin-incorporated design also allows us to calculate the effect of the angle at which the bone is placed in the resin on the stress reduction during testing. Finally, this design will allow us to change the value of bending moment. The bending moment value is based on the position of the bottom portion of the test fixture that accounts for sliding.

There are minimal disadvantages to using this test fixture. In this design, there is a possibility that it would overconstrain the bone, If the resin is too thick at the end of the bone, this could cause discrepancy in results. Another disadvantage is that the actual bone is not fixed at all points when using this test fixture. If the bone is situated in this test fixture, it would be able to rotate about one axis.

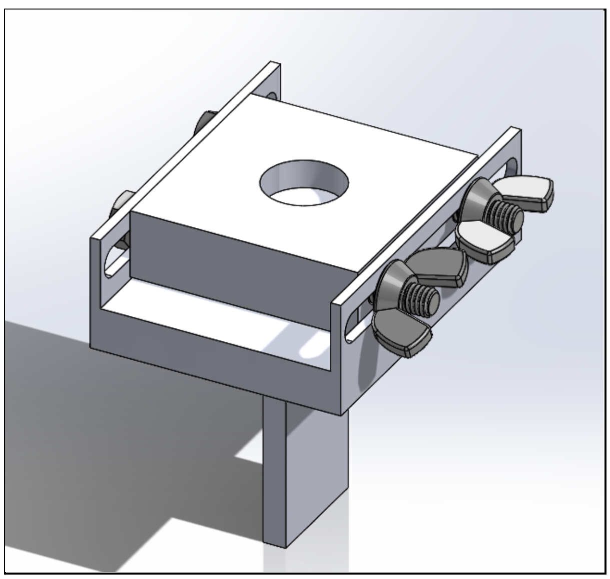

*Figure 4: Resin-Incorporated Design*

When using the resin-incorporated design, it is necessarily to establish a procedure for setting the resin. The resin thickness is an important consideration, and it should account for the variation of bone length. The angle at which the bone is placed into the resin can also affect the result of testing. Therefore, there is a need to assess the strength of the resin because the resun must not fail before the bone. Figure 5 below shows the piece for setting the bone in the resin.

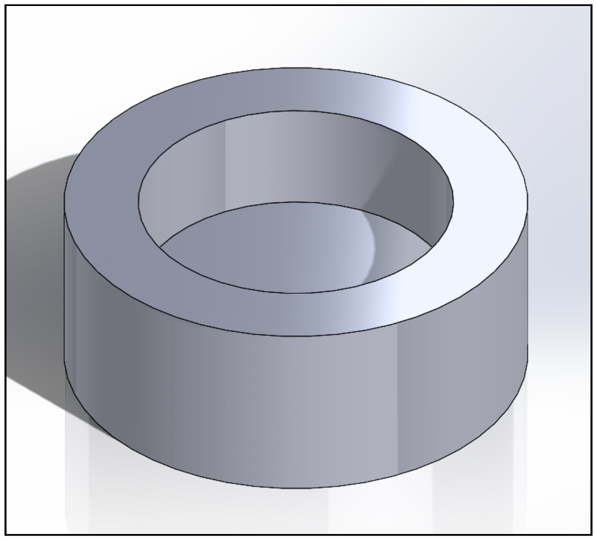

*Figure 5: Resin Setting Piece*

## *4.3 Conceptual Design*

The models created using computer aided design were evaluated before being used for rapid prototyping. Since computer aided design applications provide dimensions, constraints, and define how surfaces interface with each other, models created using the software can be replicated using a 3D printing machine. Rapid Prototyping (RP) technologies, including 3D printing, use a computer-driven, additive process to print solid three-dimensional models one layer at a time. The 3D printer available to students in the Foisie Innovation Studio is completely scalable, requires minimal set up time, and can be set up anywhere while providing a more efficient method of construction. Our model was created using polylactic acid, commonly known as PLA. It is the default filament of choice for most extrusion-based 3D printers because it can be printed at a low temperature and does not require a heated bed. The PLA models are shown in Figure 6 below.

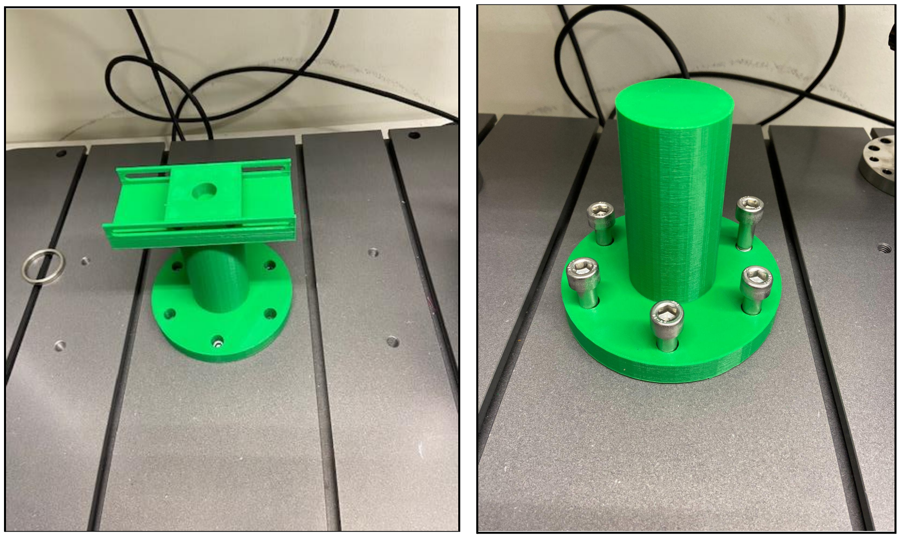

*Figure 6: Top and Bottom 3D Printed PLA Fixtures*

After 3D printing was complete, we were able to bring the model fixture into the lab. As we hoped, the model interfaced well with the machine. However, some editing must be done before moving into the final stage and before using the fixture for testing. Some of these edits include changing some of the fixture dimensions.

## *4.4 Final Design*

After the 3D model was printed, before the official parts were machined, we decided that there were some design aspects that we could modify to make it more cost effective. By making the prototype more cost effective, it allowed further modifications to be made without depleting our budget. The 3D print and solidworks models were mostly the same in the final design with modifications. After these modifications were implemented and dry runs of the test were complete, the final design was chosen and documented.

The modifications were as follows:

1. Lower the height of the bottom piece of the fixture.
2. Shorten the length of the top piece fixture.
3. Widen the fixture base.
4. Change the base shape to be more rectangular.
5. Add the screw holes to anchor the fixture only where necessary (rather than a circular pattern.)
6. Increase the diameter of the resin hole to double its current size.
7. Increase the width of the sliding resin piece outside by 75mm.

To reflect our knowledge about the adjustable overhead and reduce the amount of stock material needed, design changes were made to the sliding slot, bottom fixture, and top fixture.

Because the machine overhead could be adjusted, the bottom fixture no longer had to meet a certain height requirement and could be flush with the machine table. This was additionally advantageous because it eliminated the ability for the fixture to displace. To reduce assembly and eliminate machining threads, the sliding slot and the bottom fixture were combined into one part. The same M10 threads at 100mm PCD will be used in conjunction with M10 bolts to secure the fixture to the machine table. However, only 4 out of the original 6 clearance holes were present in the final design to keep the design rectangular. Because this fixture was only subject to compression, 4 clearance holes will provide the force necessary to secure the bottom fixture.

The top fixture was altered by decreasing the total height of the fixture and doubling the diameter of the insertion circle. Doubling the diameter of the insertion circle allowed for free movement of the bone in the X-direction when the Instron was applying a moment. This was favorable because it more realistically modeled the forces and constraints on the metatarsals during running while still offering a boundary to stop the bone from escaping from the top fixture. Components of the final design fixtures in the form of CAD models are shown in Figures 7-13 below.

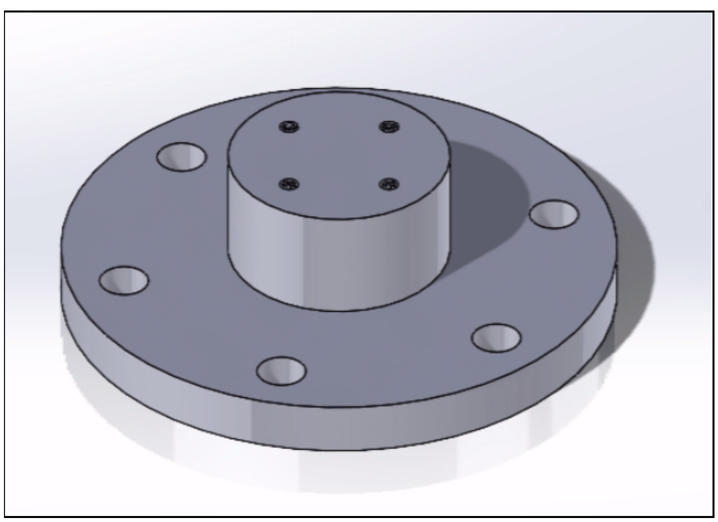

*Figure 7: Circular Bottom Fixture Design (Isometric View)*

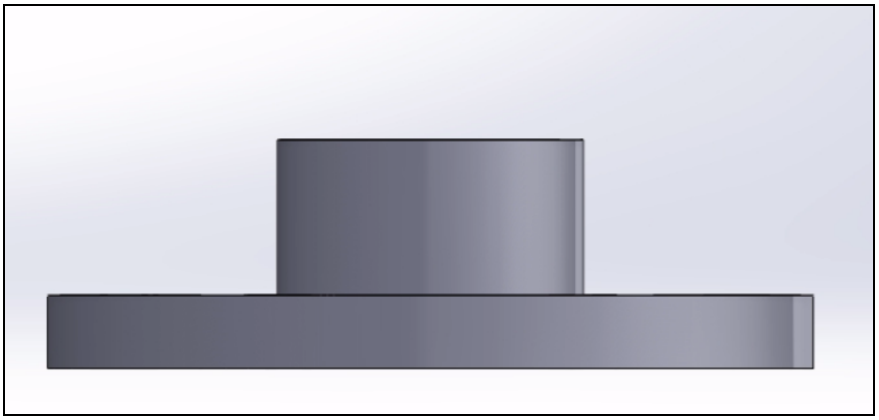

*Figure 8: Circular Bottom Fixture Design (Front View)*

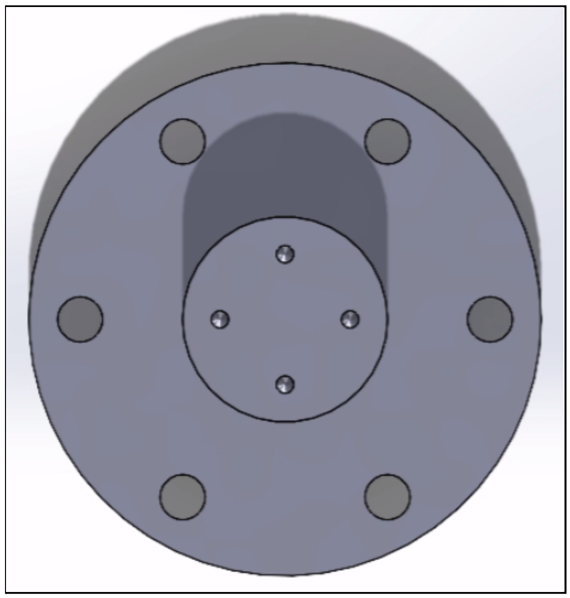

*Figure 9: Circular Bottom Fixture Design (Top View)*

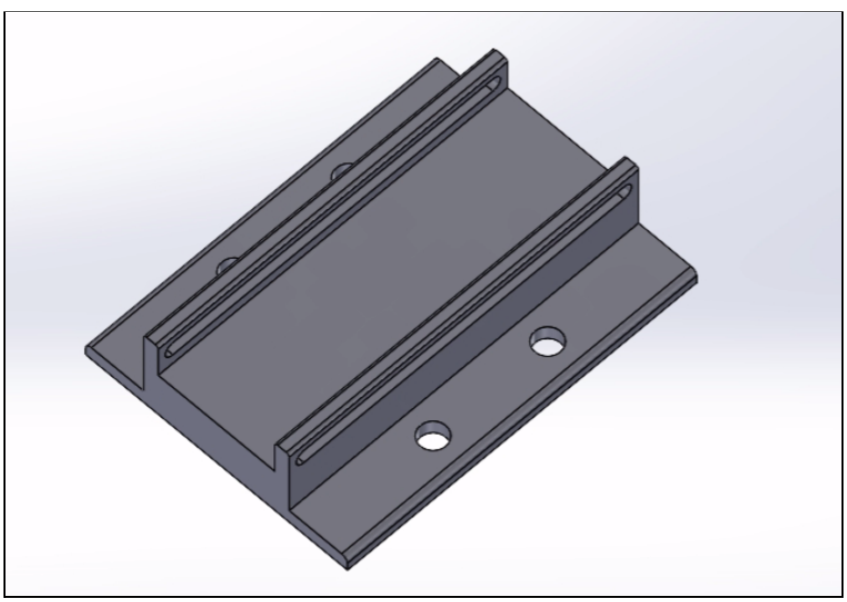

*Figure 10: Square Bottom Fixture (Isometric View)*

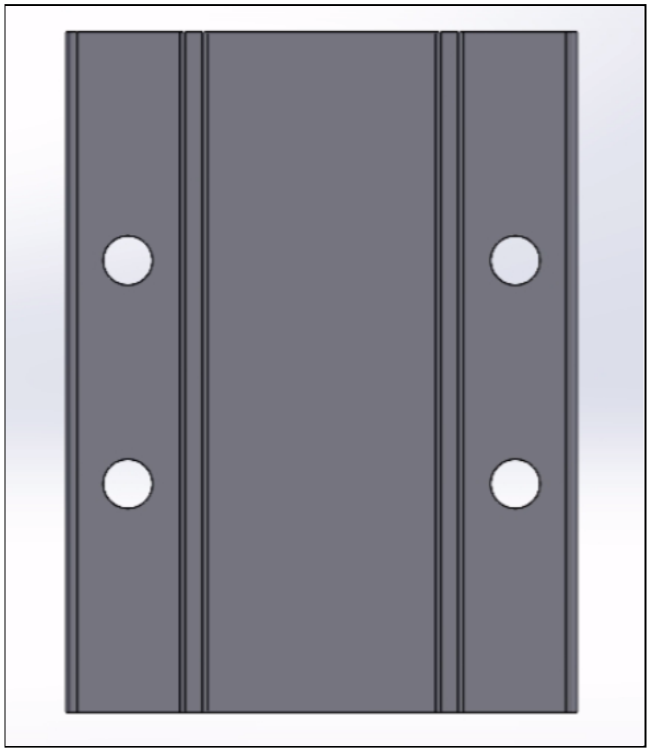

*Figure 11: Square Bottom Fixture (Top View)*

*Figure 12: Square Bottom Fixture (Right View)*

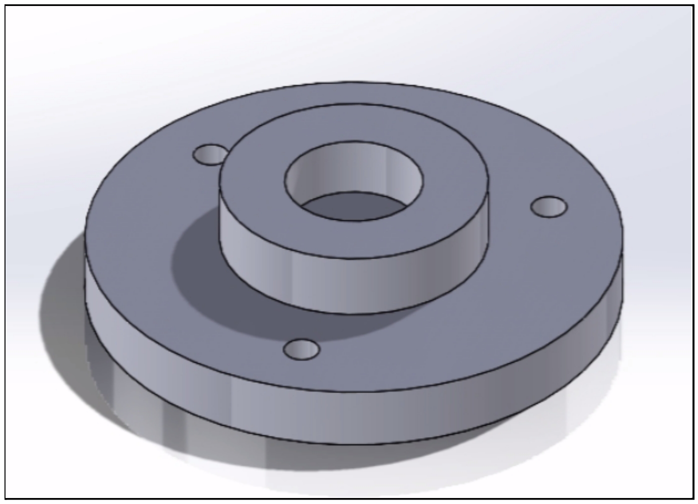

*Figure 13: Top Fixture Design (Isometric View)*

# 5. Final Design Verification

---

This chapter outlines the teams protocols and verification methods to fulfill the design specifications we outlined for our test fixture and test method. ASTM standards create an outline for the base of our testing protocol and good documentation practice. Each protocol defines a custom and constant way for every team member to execute tests that will verify the designs ability to meet the desired criteria.

## *5.1 ASTM Standard Verification*

The ASTM fatigue standards and fracture standards outline procedures, significance and scope of different processes to properly evaluate and investigate the behavior of the effects of fatigue accumulation, and in our specific case, cyclic loading impact. In particular, our protocols will reference the ASTM standard chapter E1942. This chapter is labeled “standard guide for evaluating data acquisition systems used in cyclic fatigue and fracture mechanics testing.” This standard outlines and identifies how to minimize errors when testing fracture mechanics. This distinct chapter also includes important aspects of the proper mechanical setup, error evaluation and what a proper report should include.

A mechanical testing system consists of a test frame with grips which attach to a test specimen, a method of applying forces to the specimen, and a number of transducers which measure the forces and displacements applied to the specimen. The team derived the test model from this standard by using the Instron as the testing machine, custom manufacture testing grips for metatarsal-like bones, a load cell to measure the forces, and a Bluehill method to apply the necessary forces to the bone. The team also understood the limitations of the machine as far as its error percentage, error due to noise and draft in the room, and aging of the machine and load cell.

The collection of data, both physical and technical can be divided into three parts. These include but are not limited to the mechanical test frame and its components, the electrical measurement systems and the computer processing of data. Although all of these components were carefully monitored, this specific standard chapter following is geared towards the electrical measurement system output of the transducers. The focus on this data accumulated was used to then further the understanding of bone stress injury of metatarsals, followed by a report.

The purpose of the report is to record that due consideration was given to essential performance parameters of the data acquisition system when performing a particular fatigue or fracture mechanics test. It will consist of mostly data including the measurement equipment description, waveshape and highest frequency used during the test, data rates, noise level, and the necessary details to describe these aspects.

The team will refer to the A1 section of this standard chapter to identify sources and estimation of errors including but not limited to noise spectra, data sampling errors, breaking a brittle specimen, and bandwidth. The team utilized these ASTM standards to verify that the protocols, testing, and reports are cohesive and accurately reflect the design specifications from Chapter 4.

## *5.2 Hardware Design Requirements*

Pugh Analysis to determine whether a resin-potted model was most ideal. In this analysis, two designs were evaluated against one another. Key design criterias were taken into account and weights were assigned to each. Weights were assigned on a scale of 1 to 5, 1 being of little importance and 5 being of high importance. The two models were then weighed against the criteria. The design was given a score of 1 if it allowed the criteria to be met, and -1 if the criteria would be unmet with the design. The assigned weights for each criteria were then multiplied by the -1 or 1 score for each design. All the products for each design were summed. The design with the highest summation will idealistically meet the design criteria most effectively. In this case, the Pugh analysis allowed the team to see that the resin potted model would be the best choice. This Pugh Analysis can be seen below in Table 7. The descriptions for each design consideration are outlined in Table 8.

*Table 5: Pugh Analysis  For Hardware Design*

| Criteria | Weight | Staircase Model | Resin Potted Model |
|---|---|---|---|
| Safety | 5 | 1 | 1 |
| Sizing Constraints | 5 | -1 | 1 |
| Non-Corrosive | 4 | 1 | 1 |
| Stress/Strain Relief | 3 | -1 | -1 |
| Durable | 3 | 1 | 1 |
| Precision Accuracy | 3 | -1 | 1 |
| Axial Bending Accommodation | 1 | 0 | 0 |
| TOTALS | | 1 | 17 |

*Table 6: Design Consideration Descriptions*

| Title | Descriptions |
|---|---|
| Precision/Accuracy | The testing fixture holds the specimen at the proper locations to allow for correct crack propagation and formation. |
| Stress/Strain Relief (No Preload) | The testing fixture allows for stress/strain relief. |
| Sizing Constraints for the Machine | The testing fixture shall not exceed the diameter, length, and width of the testing machine. |
| Safety | The testing fixture shall not inhibit the safety features in place on the testing machine. |
| Durable | The testing fixture can withstand multiple tests in a row. |
| Non-corrosive | The testing fixture material allows for hydration of the specimen. |
| Axial Bending Accommodation | The testing fixture accommodates for cyclic axial loading as well as cyclic axial loading and bending. |

## *5.3 Verification Testing*

### 5.3.1 Hardware Verification Testing

The first iteration of custom-designed fixtures were designed in accordance with the Pugh Analysis described previously. For the fixture material, 6061 aluminum will be used. 6061 aluminum alloy is a precipitation-hardened alloy that contains magnesium and silicon. 6061 aluminum alloy was selected due to its excellent joining characteristic, and acceptance of applied coating. In addition, it combines relatively high strength, good workability, is resistant to corrosion, and can be purchased at a relatively low cost.

In order to ensure the custom-designed fixtures interfaced properly with the Instron E3000 Electropuls, 3D printed polylactic acid (PLA) models of the parts were printed. These models were manually installed in the Instron E3000 ElectroPulse. All tolerances and dimensions were printed as expected, as seen below in Figures 14-15.

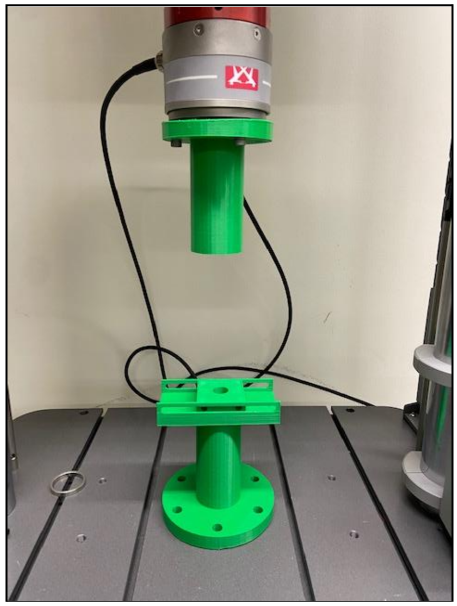

*Figure 14: 3D Printed Parts Installed in Instron ElectroPuls*

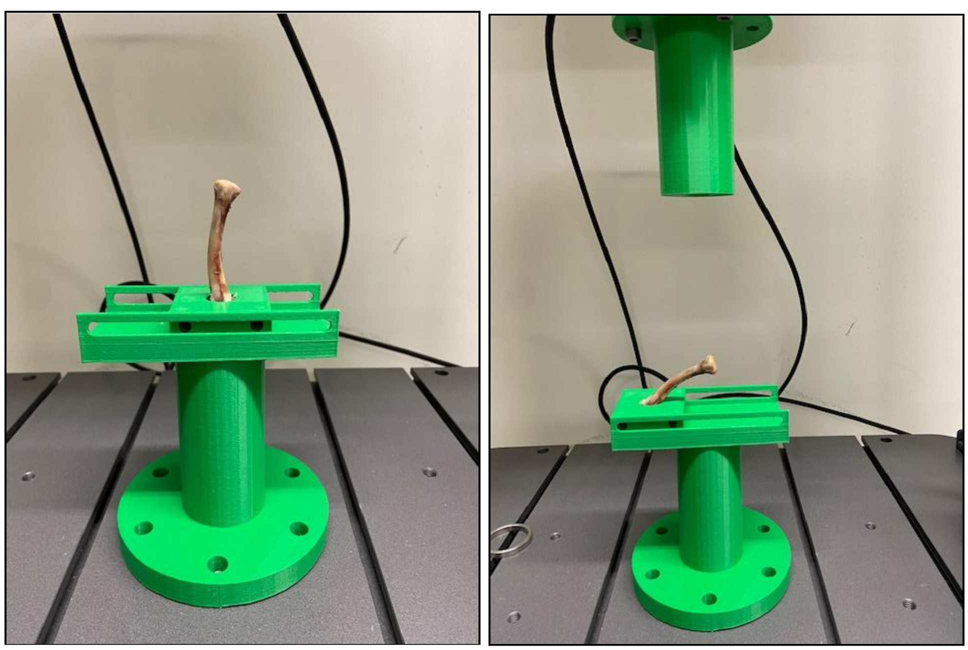

*Figure 15: 3D Printed Parts Containing Bone Specimen*

However, this iteration of the design was made assuming the Instron's overhead could not be adjusted. After learning the overhead could be adjusted, the group designed a second iteration of custom-made fixtures. In this iteration, the bottom assembly was flush to the bottom of the table and incorporated the sliding slot and bottom piece into one part. This eliminated the chance of unnecessary displacement at the extremes of the sliding slot and reduced the amount of parts in the assembly. Additionally in this iteration, a bone securing piece was added to stop the potted bone from levering out.

The second iteration of fixtures were fabricated using the CNC machines in Washburn Shops. In order to generate the CNC code, Esprit, a CAM solution for machining applications, was used. Solidworks part files were imported into ESPRIT and then tool paths, feeds, and speeds were defined to cut the stock material using part features, such as edges or holes. Using the software, users are able to simulate the machining of the part on both the lathe and minimill. Both the lathe and minimill were used to manufacture the top fixture. A lathe was selected for machining the outer profile of the top fixture because it is best suited for machining rounded or circular parts. Then, the minimill with circular jaw was used to face off the unwanted material on the back side of the parts and create the clearance holes. For the top fixture, a 4" diameter cylinder of 3” length was ordered. For all other parts, only the minimill was used. For the sliding slot part, a 2" thick by 5" wide by 6” length block was ordered. For all other pieces, because they were relatively small, stock material was gathered from the existing supply in the machine shop. Once the parts were fabricated, they were assembled and placed on the Instron. Photos of the machined parts on the Instron can be seen below in Figures 16 through 19.

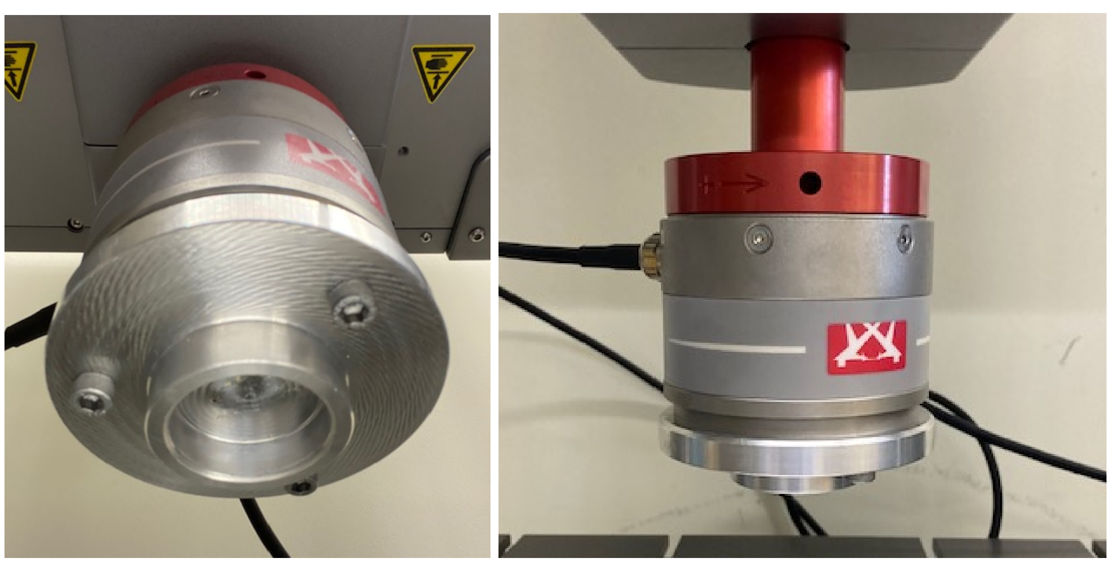

*Figure 16: Top Fixture Attached to Instron Actuator*

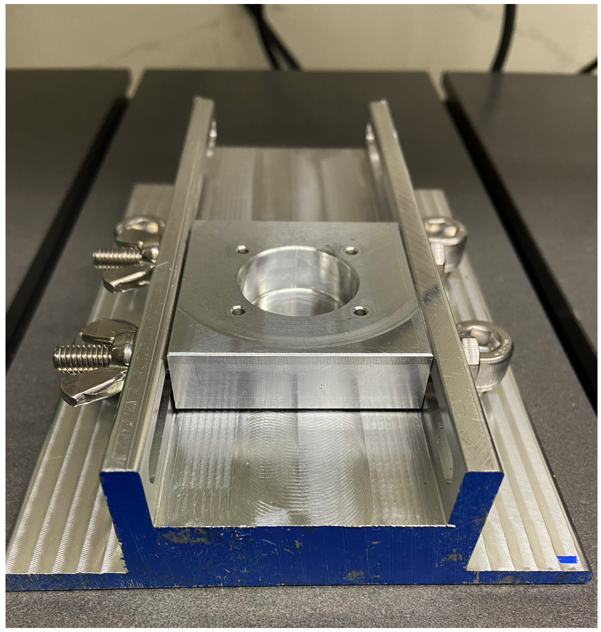

*Figure 17: Bottom Fixture Front View*

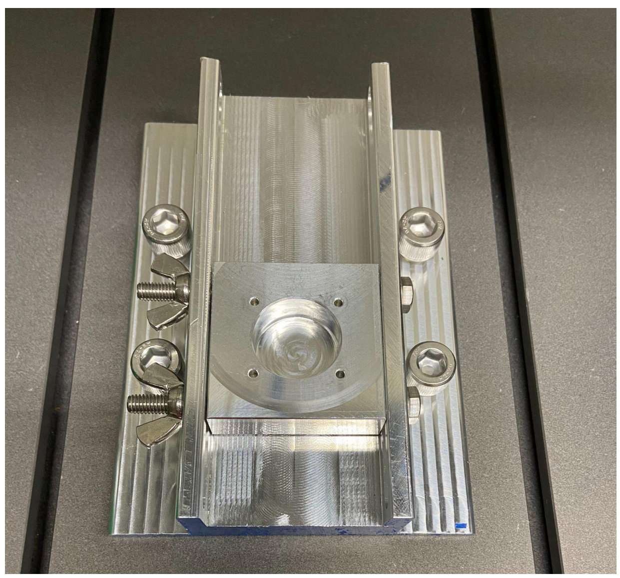

*Figure 18: Bottom Fixture Top View*

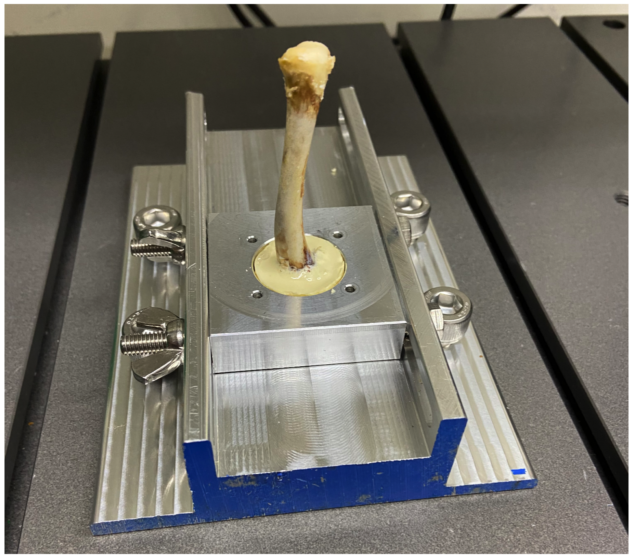

*Figure 19: Bottom Fixture with Potted Bone Front View*

**5.3.2 Software Verification Testing**

*Instron Dynamic Software*

Interface with the Instron E3000 ElectroPuls requires the computer Instron Dynamic Software: Bluehill WaveMatrix and Instron Console. In this software, specific methodology can be created to guide the testing process. WaveMatrix allows the user to customize the test method to prompt the production of ideal results. To understand the functionality of this program, the team constructed a series of troubleshooting tests. Using the 3D printed PLA testing fixtures, the team performed compressive tests on a rubber stopper.

The team instructed the load cell to compress a rubber stopper until a force of 75 N was experienced by the load cell. The load cell was instructed to move at a rate of 3 Hz and maintain a sinusoidal pattern. We instructed the load cell to complete three sets of identical tests, each containing 20 cycles. Unfortunately, the extension of the machine was unable to be zeroed. Due to this, we believe the amount the load cell could extend was limited. Therefore, the load we instructed the load cell to read was unachievable. The results of the test, even though they are not to the ultimately desired load, depict a sinusoidal fatigue rhythm. The results are shown in Figure 20 below.

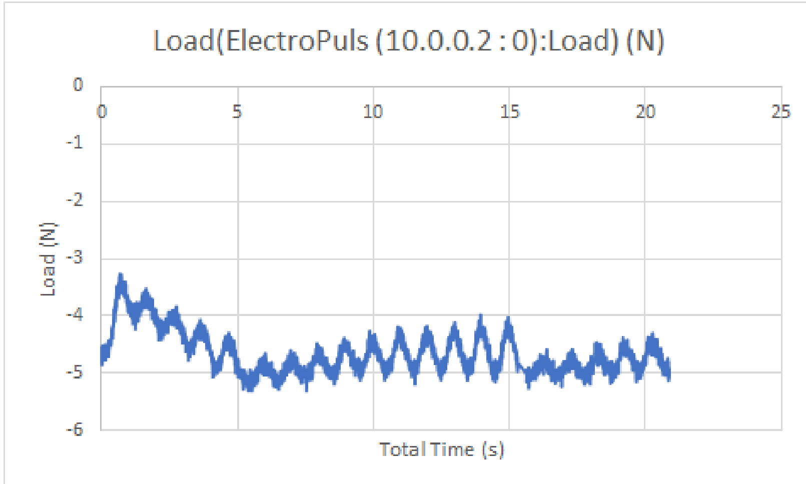


*Figure 20: Load (N) vs. Time (s) of Preliminary Testing; Rubber Stopper was compressed to observe if the test method could function in the desired manner.*

Although this test will not be representative of the data we aim to collect in avian bones, it allowed the team to gain knowledge on the abilities and limitations of the Instron E3000 ElectroPuls. From the data, we are able to distinguish the sets of cyclic loading and verify that these will be completed as instructed. Completing these tests with our 3D printed PLA models enabled the team to see how our fixture models reacted with the machine in motion. Although they were not yet in the desired material, the team observed that the dimensions and overall design would function appropriately for the testing procedure.

### 5.3.3 Mechanical Verification Testing

Before testing could begin, all students made sure to wear adequate protective equipment (PPE) in the laboratory including safety goggles and close-toed shoes. Students ensured that the work area was inspected and did not contain any debris or improper lighting. Manual controls were also checked for proper functioning, ensuring that the crosshead was in the correct position. Proper function of the emergency stop switch was also checked. Once laboratory safety was ensured, testing could begin.

All testing was done using an ElectroPuls E3000. The E3000 is an all-electric test instrument designed for dynamic and static testing. The machine includes a load cell, console software, and tuning based on specimen stiffness. The crosshead lifts are also electrically operated. In contrast with other machinery, the E3000 is powered from a single-phase supply that requires no additional utilities such as pneumatic air or hydraulics for basic machine operation. An E3000 technical drawing with dimensions is shown in Figure 21 below.

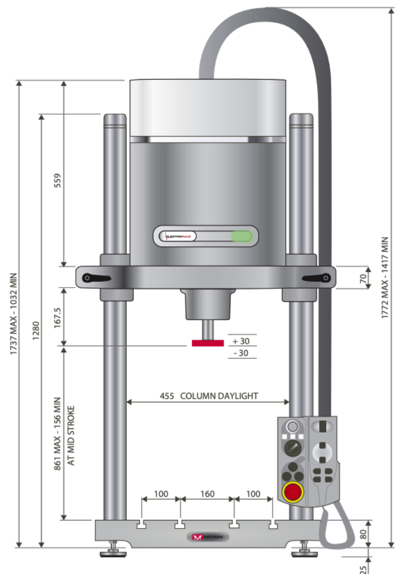


*Figure 21: Instron E3000 ElectroPulse front view with dimensio*ns

The mechanical testing protocol using the E3000 is as follows:

1. Secure 3D-printed fixtures into the machine.
2. Screw top and bottom fixture pieces into the base and load cell of the machine.
3. Open Instron Console program and Instron Bluehill WaveMatrix Program
4. Manually adjust load cell to specified height, allowing the machine to extend to the desired depth.
5. Separate top and bottom fixtures by the approximate length of the bone specimen.
6. Balance the load cell using the Instron Console Program.
7. Use measurement data from CT scanned images of bones to calculate the amount of desired force.
8. Once the desired force has been calculated, adjust the sequence of the Bluehill WaveMatrix software to incorporate an amplitude equal to the desired force.
9. Adjust the advanced amplitude control on Bluehill Wave Matrix software by inputting a maximum load of the desired force and a minimum load of 0 N.
10. Carefully place the bone specimen in between the two fixtures on the E3000.
11. Apply a 5 N tare load to the specimen.
12. Use the Instron Console program to zero the extension (digital position) of the load cell.
13. Begin the test on the Bluehill WaveMatrix Program.

14. Allow the test to run until the number of interactions is complete (or until the end of test criteria is met).
    a. If there is a 10% force reduction in the specimen, this signifies the beginning or injury and the test can be concluded.
15. Once the test is complete, carefully remove the safety shield.
16. Before removing the specimen, ensure that all other group members and laboratory persons cannot operate any of the system controls.
    a. Keep clear of the jaws of a grip or fixture at all times.
    b. Keep clear of the hazard area between the grips or fixtures during actuator or crosshead movement.
17. Ensure that all actuator or crosshead movements necessary for installation or removal are slow and, where possible, at a low force setting.

### *5.4 Specimen Preparation*

Dissecting chicken legs gives us the opportunity to observe and probe internal structures that resemble those in our own bodies. Chicken legs have parts that are easy to examine and work with, and the skin comes off easily using the correct technique. The dissected chicken bones are shown in Figure 22 below. The correct technique for chicken dissection is as follows:

1. Gather all materials: raw chicken legs, scalpel, tweezers, gloves, and safety goggles.
2. Reach inside of the hip with the end of your fingers and pry the skin free from the underlying periosteum.
3. Gradually peel the skin inside out off of the ankle end. The thigh and drumstick will be revealed.
4. There will be a tough band of cartilaginous material around the ankle, which contains passages through which tendons slide. Carefully cut the cartilage with the scalpel and pull it away from the bone.
5. Gradually pry, squeeze, or pull apart the muscles until finding the drumstick. The drumstick will appear as a bundle of muscles, each of which has its own tendon that runs out to the foot.
6. Carefully remove and pull back the skin and muscles surrounding the bone using a scalpel and tweezers.

7. Once a sufficient amount of muscle has been removed and the bone is revealed, the skeleton of the chicken leg will be apparent. The bones of the chicken leg are the hipbone, femur, kneecap, fibula, and tibia.
    a. The thigh contains a single large bone, the femur.
    b. The lower leg contains a pair of long bones, one long and strong (tibia) and one thin and frail (fibula).
    c. The fibula will appear as a needle structure sticking down from the knee joint.
8. Discard the skin and muscles in the proper waste basket.
9. Gather all chicken bones to be cleaned and stored in the freezer.

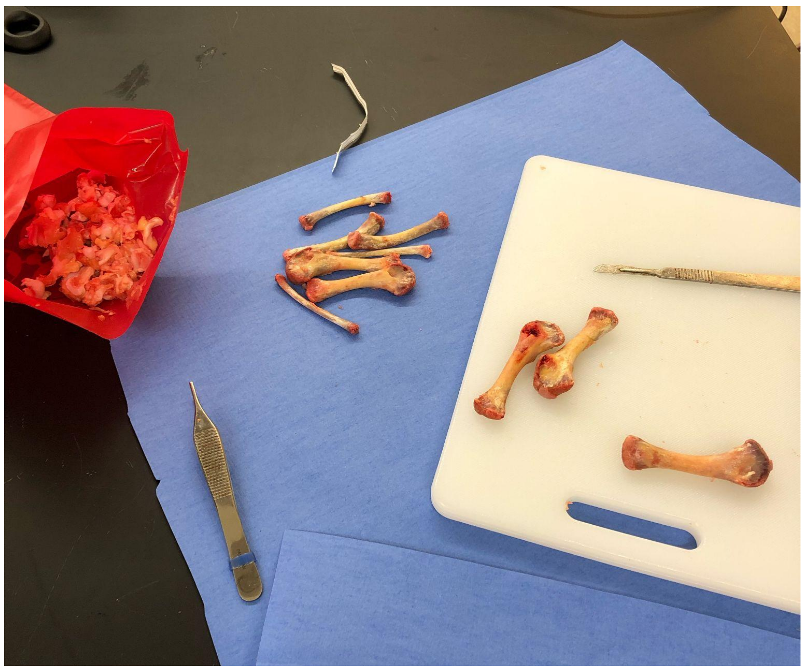

*Figure 22: Dissected Chicken Bones*

Once all chicken bones have been dissected, they are prepared as biological samples. Bones should be prepared using personal protective equipment including gloves, a lab coat, and safety glasses. Before beginning the protocol, students collected the dissected chicken bones, small plastic ziploc bags, one large ziploc bag, saline solution, gauze, aluminum foil, and a plastic container deep enough to fit a chicken bone and have it fully submerged. Bones are preserved by being kept frozen. Freezing the bones matintans most of the mechanical properties, only resulting in slight changes in the stiffness of the sample. If the bones were not frozen, the specimen would degrade and lose their strength and structure. All bones should be thawed in a room temperature saline solution for around one hour and wrapped in saline soaked gauze until it is time for testing. It is important to keep the bone specimen during all stages of preparation. Wrapping the specimen in saline soaked gauze effectively keeps the bone in an environment with 100% humidity. The complete fresh-frozen protocol is as follows:

1. Label all ziploc bags with the following:
    a. Group name and contact information
    b. Date that specimen was placed in the biohazard freezer-date when bones are removed from the freezer
    c. Specimen Type - Chicken Leg
    d. MQP - Team Name - Advisor
2. Take a plastic container and fill ½ with saline solution.
3. Cut enough pieces of gauze and aluminum foil to cover each chicken bone sample.
4. Remove soft tissue from fresh chicken bones using the protocol above.
    a. Be sure to remove all soft tissue and the layer of fascia covering the bone surface (periosteum) without damaging this outer boney layer
5. Place the cut pieces of gauze into the saline solution, making sure that the gauze is fully saturated. The gauze should not be dripping wet.
6. Wrap each sample from top to bottom using the saline-saturated gauze.
7. Cover each gauze-wrapped sample in aluminum foil.
8. Place each of the aluminum wrapped specimens into the small, labeled ziploc bags.
9. Place each small ziploc bag that contains a wrapped specimen into the large labeled ziploc bag.
10. Place the large labeled ziploc bag into the biohazard freezer.
11. Dispose of all biological waste.
12. Dispose of all blades in the sharps container.
13. Wash all tools with amphyl solution in the laboratory sink and place each tool into the white container located next to the sink.

## *5.5 Image Processing Data Collection*

### 5.5.1 Materialise Mimics

Once the specimen was cleaned and prepared, we collected the dimensions to verify the bone length, diameters, and overall size was as close to a human metatarsal as possible. To do this, each specimen was scanned by the CT scanner and uploaded to a software called Materialise Mimics. Materialise Mimics is a software for 3D design and modeling developed by a Belgian company, Materialise NV. The characterizing and segmenting anatomy features were used to identify landmarks and measurements of the avian specimens. [Materialise mimics, n.d.]

The CT scan results of five different bones are shown in Figure 23, below. The protocol is as follows:

1. Follow the dissection bone protocol for fresh frozen bones located in Section 5.3.
2. Estimate using a caliper if the dimensions of the specimen are within range of human metatarsal.
3. CT scan the specimen.
4. Upload the Dicom files onto the Mimics platform to gain the Mimics file type.
5. Collect and analyze the values returned from the mimics file.
6. Retrieve the Dicom files of the specimen.
7. Upload the respective files to a drive for future use in other image processing programs.

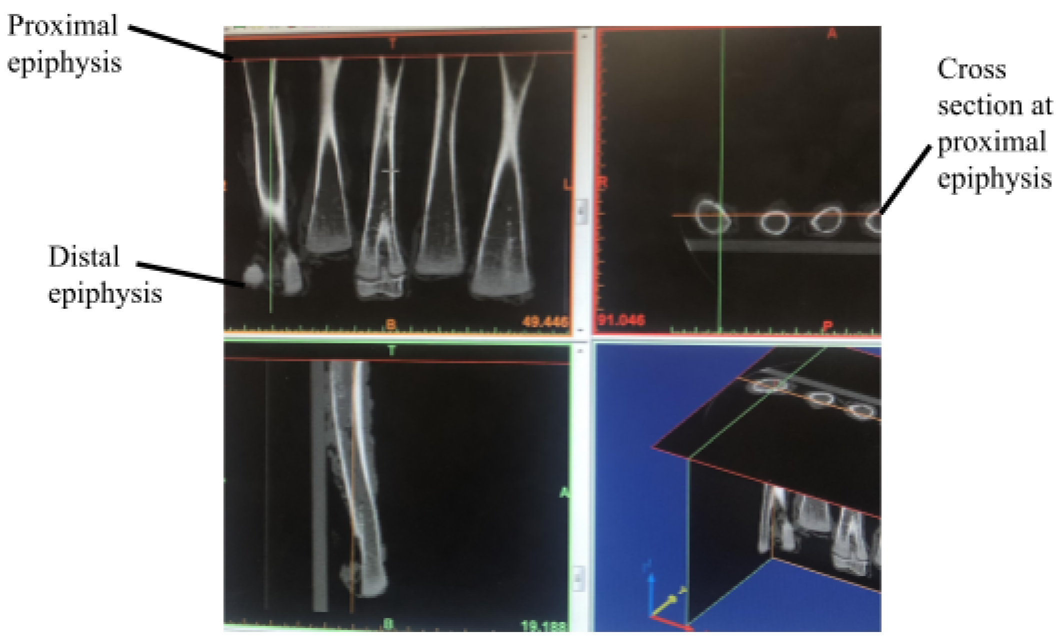


*Figure 23: CT Scans of Five Avian Tibia Specimens*

The Mimics program allowed us to get transferrable images for input into future software programs. The bone labels, lengths, midpoints, cross sections, and DICOM images can be referenced in Appendix E. Additionally, we obtained the transferable images of the midpoint cross section of each individual bone. These were pivotal for determining cross sectional area and use of the VA-BATTS program for further analysis.

### 5.5.2 VA-BATTS

VA-BATTS is a plane-strain finite element model. This Matlab-based tool is used to calculate bending, axial, torsional, and transverse shear stresses within bone cross sections that have inhomogeneous material properties [Kourtis, 2008]. The density of the bone shows as the gray value of the image in this software and it is related to the stiffness of the bone. By taking the irregular cross section and irregular density, the software will divide them into elements that have a location and assigned modulus based on that density. In the first section of the code, the loads are specified. By altering and inputting unique values into the code, a load can be simulated and applied to the bone of interest. The first section of code "0. Input" allows the user to input values for flexural load, three-point bending, axial loads, and torsion displacement.

```
%% 0. INPUT

% Flexural Loads
Mx              = 0;              %in N.m
Mx=Mx*1000;
My              = 0;              %in N.mm
% OR (3pt bending)
Qx              = 0;            %in N
Qy              = 0;            %in N
z_pos           = 1;            %in mm
% Axial Loads
P               = 201.2581323;            %in N
            T              = 1;
T=T*1000;
% Torsion displacement
```

*Figure 24: First section of code: '0. Input'*

The VA-BATTS code, main.m, is opened by either typing "main.m" or opening the Matlab file and clicking on the Run button. This main code calls other functions based on inputs. A flow diagram for the code can be seen in Figure 25, below.

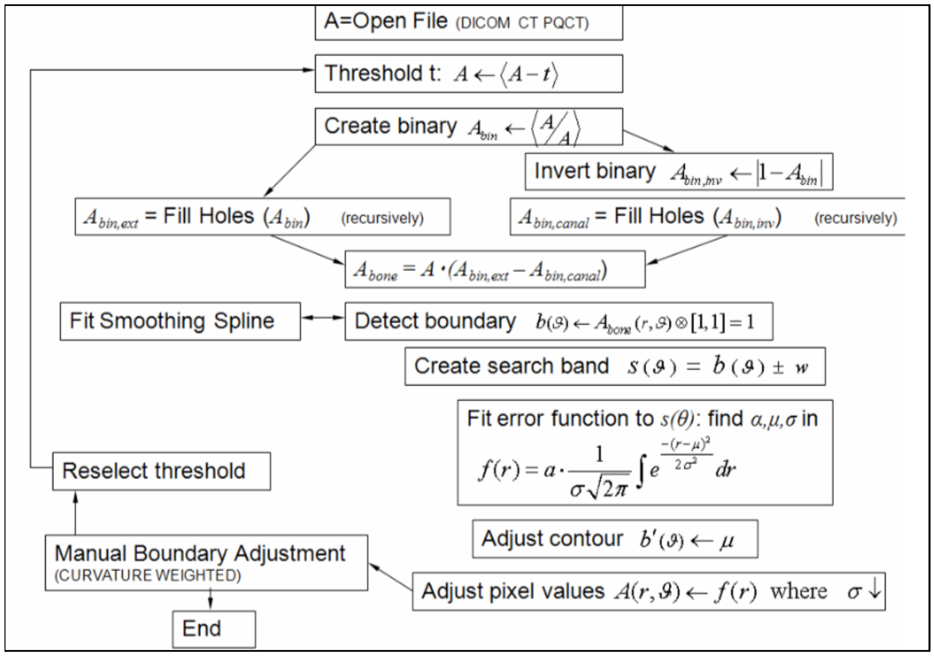


*Figure 25: Flow Chart of VA-Batts code*

Once the user inputs the desired applied loads and the code is run, the file selection dialogue will appear. The DICOM files transferred from Mimics are compatible with this software and are to be opened in the program pop up. The software will then prompt you to crop the image so that it only shows the region of interest. Following the crop, a mesh type selection dialogue will appear and ask whether the mesh type should be solid or donut. In the case of a hollow bone, the donut shaped mesh generator is triggered. Once the mesh type has been selected, the program will calculate the allowable thresholding levels. A second version of the original image will appear to the right of the original image. The bone will be contoured by a blue spline whose control points are marked as dots and will be used as mesh seed points. The contour spline can be altered by the user. Once it satisfactorily prescribes the bone, right clicking in the left window will confirm the contour spline selection and allow the program to continue to the next analysis step. From there, the program will calculate and report the cross sectional properties and the dresses given the load case without user interference. In order to calculate bending, beam theory is employed to calculate the normal stresses throughout the cross section. These calculations take place at the centroid locations and are then averaged across the element boundaries to produce continuous plots.

The main goal of using the VA-BATTS software is to solve this finite element problem and determine the stresses throughout different loading conditions of bones. Once this process is completed and consistent in avian tibia, it can be applied to human metatarsals as well.

The tutorial allowed the user to become familiar with the program inputs and analyze the bone stresses presented by the program. The tutorial allowed understanding through uploading and analyzing DICOM images of a midshaft of a femur. By following the previously stated procedure, the program can calculate and report the cross section properties and stresses, in MPa, given the load case. In Figure 26, reading from the top left to bottom right image, the images are the original image, the cropped and thresholded image, the trabecular and cortical image, the shear stress image, and the out of plane bending stresses.

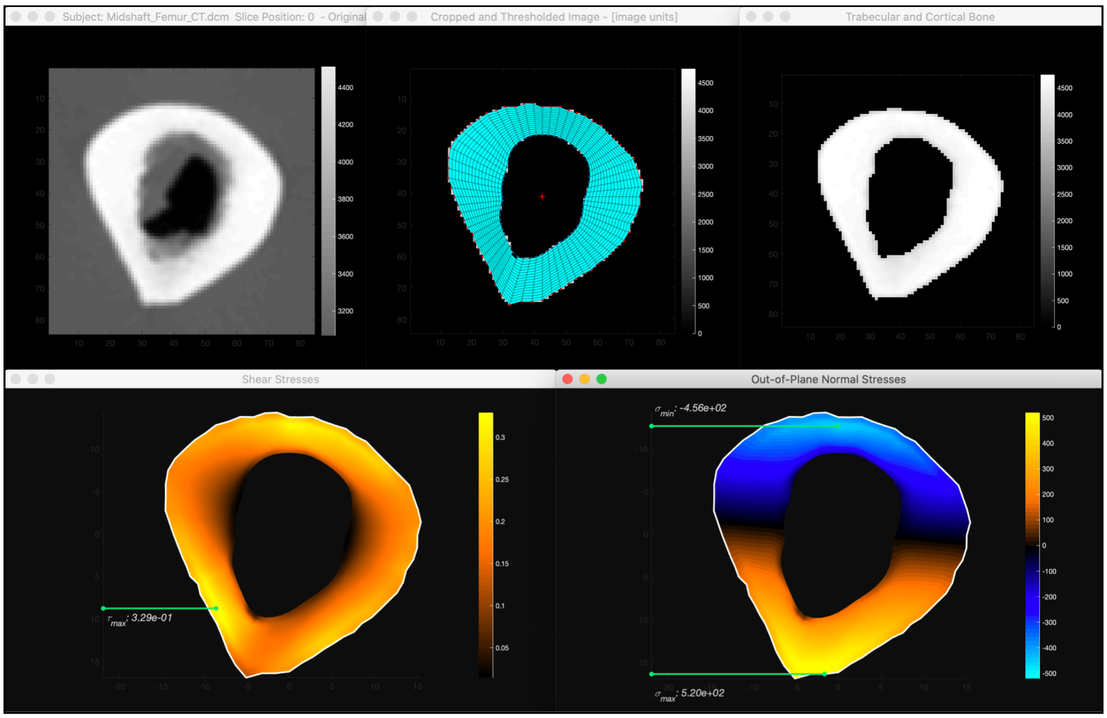


*Figure 26: Program Example of Midshaft of Femur*

Once the basic function and inputs were understood, the DICOM files from our avian specimen could be integrated into the VA-BATTs software. We added an axial load associated to the each avian tibia, values shown in Table 14, and ran the software as previously stated. The result of this applied axial load can be seen in the images and values below.

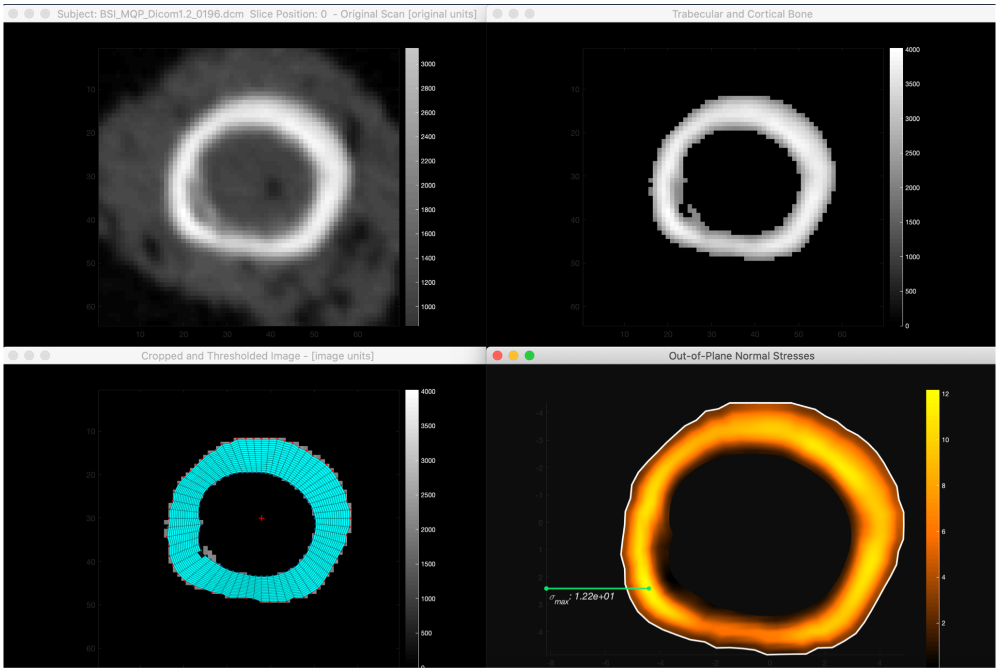


*Figure 27: Axial Loading Conditions in Avian Specimen*

The above images show the original DICOM cropped image, the trabecular and cortical bone image, the cropped and thresholded image, and the out-of-plane normal stresses. The most important data is the out-of-plane stress value. It is evident that this bone is being loaded under axial compression, because the maximum stresses are constant along the cross-sectional area.

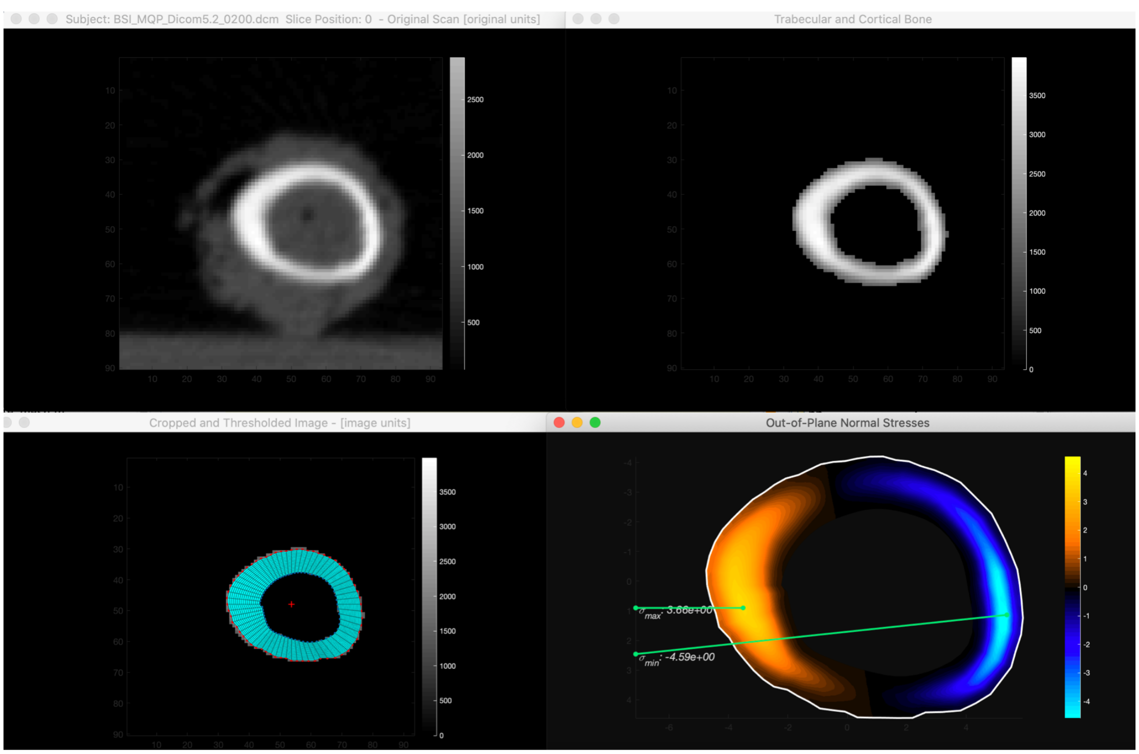


*Figure 28: Bending Loading Conditions in Bone*

The above images show the original DICOM cropped image, the trabecular and cortical bone image, the cropped and thresholded image, and the out-of-plane normal stresses. The most important data is the out-of-plane stress value. It is evident that this bone is being loaded in bending, as the orange color, which represents the maximum stress, is on one side of the bone, while the blue color, which represents minimum stress, is on the other. This differentiates where the bone is acting under tension or compression. Future research with bending loading condition conditions will provide the group the opportunity to best replicate physiologically relevant running conditions. Thus, understanding the use of bending within the context of the software will be of great value and usage for future testing on both avian specimens and human metatarsals.

## *5.6 Potting Specimen Bone*

This bone potting specimen protocol defines a common system in which we will be testing our samples. Following this protocol verifies the legitimacy of the system in each sample, as it allows for a constant verification that the samples are being prepared the same for each test. Four potted bones are shown in Figure 29 below.

### 5.6.1 For Axial Bending Test

1. Place a paper cup on scale and zero the scale.
2. Add 7g of Side A Resin into the paper cup on the scale using a pipette.
3. Add 7g of Side B Resin into the paper cup on the scale using a pipette.
4. Stir rapidly for 30 seconds.
5. Using a paper towel or cue tip, coat the inside of the potting mold with a very thin layer of Vaseline.
6. Place the specimen into the resin in the potting mold straight-up, vertically at 0 degrees.
7. Pour the resin in the potting mold around the specimen.
8. Hold the bone vertically until the resin has turned an opaque yellow and the bone is firmly held in place at 0 degrees.
9. Allow the bone to rest in the resin for 12 minutes.
10. Pull the resin out of the potting mold using small circular motions while holding the bone.
11. Wrap the remaining bone sticking out of the resin in gauze soaked in saline.

12. Put in a ziploc bag and back into the refrigerator for 24-36 hours to let the resin fully set.


*Figure 29: Potted Bones A-D*

Figure 29 identifies 4 different specimens throughout different potting procedures. At first, each resin part was measured using equal parts of 11mL each. Specimen's A and B show the result of this type of procedure. An equal volume procedure resulted in lots of bubbles and an overflow out of the potting mold as the resin began to set. The resin never actually fully sets and the results are gummy paste. Specimen's C and D show the results of the procedure 5.6.1 above, in which the parts of resin have equal weights. This procedure results in a strong and full set of the resin with no air bubbles and a rock-like exterior. The bone is unable to slip out of the resin in specimens C and D. Any alterations of the 5.6.1 procedure can be made above as long as each Side A and Side B of the resin are kept at equal weights.

## *5.7 Specimen Hydration*

As specified by the design constraints listed in the client statement, the bone must remain hydrated in saline throughout the duration of the test. Because there will likely be many cycles of loading being performed by the Instron, tests will take numerous hours. The group wanted to invent a method to automatically hydrate the specimen so that members of the group did not have to be present in order to hydrate the specimen. To do so, the group plans on using a stepper motor controlled by an Arduino to provide the forces necessary to simulate a hand squeezing a spray bottle twice every hour. Once developed, we will place the Arduino assembly containing the spray bottle at an optimal distance and angle from the specimen. When triggered by the motion of the motor, the bottle will spray the gauze-wrapped specimen with the saline solution.

Because we are performing many loading cycles on the test bones, we anticipate testing will take up to 20 hours. For this reason, we developed an automated spray bottle system to keep the bone saturated in the saline solution throughout the duration of the test. The automated spray bottle assembly will be used when group members are not physically in the lab to spray the saline solution themselves. The components of the assembly are an Arduino Uno, a small DC motor, a mechanical lever, a custom-made plastic bracket, and a spray bottle. Operation of the automated spray bottle system will occur once every half hour. When triggered, the DC motor will spin to create a displacement with the mechanical lever, which then exerts a force on the handle of the spray bottle and causes it to spray the saline solution inside. Exact timing and forces are currently to be determined.

### *5.8 Testing Preparation*

Once hardware machining was complete, testing could begin. In order to set up the test, input values needed to be designated for the bluehill software. One option for testing was to keep the force standard for each bone tested, and the other option was to keep a standard strain and alter the force according to the size of the bone. Although keeping force consistent would allow the input value in the bluehill software to stay consistent, controlling the metric strain computation gave the advantage of allowing for individual variation between bones. One disadvantage to keeping the force consistent across a variety of bones is that applying a fixed force to each bone would systematically apply a higher strain on smaller bones than it would on larger bones. Therefore, the decision to adjust the applied for so that the same target strain was accomplished regardless of bone size was reached. This approach allows control over variables such as area, load, number of cycles, and type of testing.

The chicken bones used for testing were irregular and varied in size. Due to the non-uniform shape, the bones also experienced bending during load conditions. The cross sectional area of the bones was most uniform and smallest at the midpoint of the bone. The midpoint had the smallest second moment of area as a function to size and achieved the highest stresses. According to the strain history of bone, peak strain maxes out at 300 microstrain [Fritton, 2000]. Establishing a strain value allows further calculation of stiffness. When a load is applied to the bone, deformation can be measured. Stiffness is the quotient of the force in newtons and deformation in meters. As the deformation increases, the stiffness will decrease.

When plotting the applied force versus displacement throughout loadinging cycles, the displacement increased over time.

Fatigue testing can be a timely operation. If the goal is to reach a small value of stiffness, increasing the force will decrease the test duration. Conversely, doubling the number of cycles in an allotted amount of time will allow the stiffness reduction to be reached quicker. On an S-N curve, stress is plotted over the number of cycles completed. The stress values represent the peak to peak measurement. Over time, the curve will exponentially decrease by the power of 10, as seen in Figure 30 below. The goal with each specimen is to reduce stiffness over time before reaching failure. There will be biologic variability among specimens.

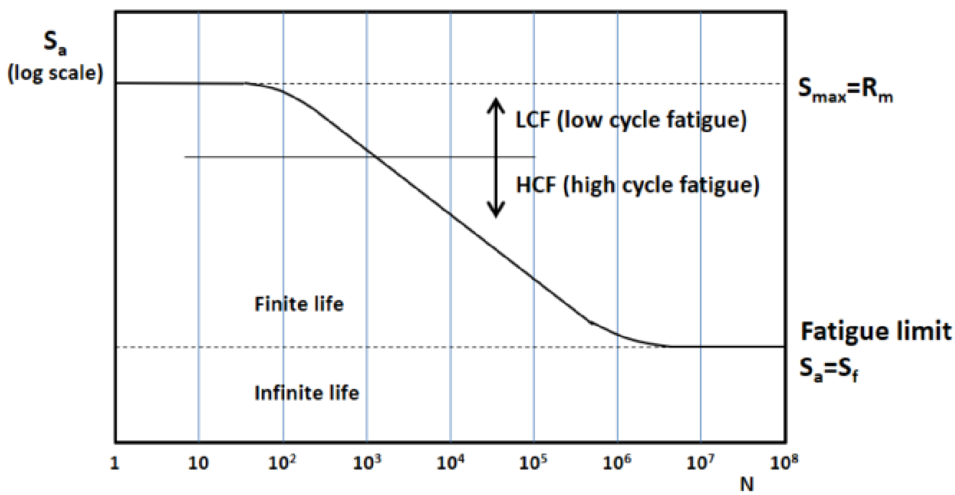


*Figure 30: Standard S-N Curve*

# 6. Design Verification Discussion

---

## *6.1 Preliminary Testing*

Preliminary testing with machines fixtures began on March 8th, 2021. During this stage, cooked bones or varying sizes were used as test specimens. Cooked bones were used at this stage because they were potted in resin and we were able to utilize CT scan data available for each of the bones. Although the cooked chicken bones do not simulate the native chicken bone, the goal at this stage of the process was to troubleshoot with force values using the design fixtures and Instron machine. During this day of preliminary testing, six different tests were conducted, In each of these tests, the strain remained constant. A 50 N force was applied to five out of the six bones, as seen in Table 9 below. The frequency in each test varied from 2-3 Hz. Variance in frequency allowed the group to analyze the effect of this variable on the overall test.

*Table 7: 3/8/21 Preliminary Testing Data*

| Bone # | Modulus of Bone (N/m$^2$) | Strain | Cross Sectional Area (m$^2$) | Applied Force Necessary F=.003AE | Cycles | Frequency |
|---|---|---|---|---|---|---|
| Mini Bone #5 | 17000000000 | 0.003 | 3.0190 * $10^{-5}$ | 1539.7 | 3600 | 3 Hz |
| Cooked, No Label 1 | 17000000000 | 0.003 | N/A | 50 | 3600 | 3 Hz |
| Cooked, No Label 2 | 17000000000 | 0.003 | N/A | 50 | 3600 (236 before error occurred) | 3 Hz |
| Cooked, No Label 2 | 17000000000 | 0.003 | N/A | 50 | 3600 | 2 Hz |
| Cooked, No Label 3 | 17000000000 | 0.003 | N/A | 50 | 3600 | 2 Hz |
| Cooked, No Label 4 | 17000000000 | 0.003 | N/A | 50 | 3600 | 3 Hz |

### 6.1.1 Troubleshooting - Frequency and Method Functionality

Out of the six tests ran on the first preliminary testing day, the test completed on the second cooked bone provided the most useful data. Instead of applying a calculated force value, this test was given a set 50 N end-of-cycle value to observe the cycling of the test. The test was set to include 3600 cycles (1 cycle=downward and upward stroke) but exhibited an error after cycle 236. The test ran at a rate of 3 Hz (.165 s for the downward stroke, and .165 s for the upward stroke). The group determined that 3 Hz was not enough time to achieve the force value of 50 N, as it only cycled between 13 and 32 N. The cross-sectional area was not measured in this test as it did not determine the force we planned on applying. The preliminary testing input values for this test are shown in Table 10 below. Figure 31 below shows the output force values obtained during the first thirty seconds of the test.

*Table 8: Cooked Bone #2 Input Measurements (3/8/21)*

| Bone # | Modulus of Bone (N/m$^2$) | Strain | Cross Sectional Area (m$^2$) | Applied Force Necessary F=.003AE | Cycles | Frequency |
|---|---|---|---|---|---|---|

| | | | | | | |
|---|---|---|---|---|---|---|
| Cooked No Label 2 | 17000000000 | 0.003 | N/A | 50 | 3600 | 3 Hz |

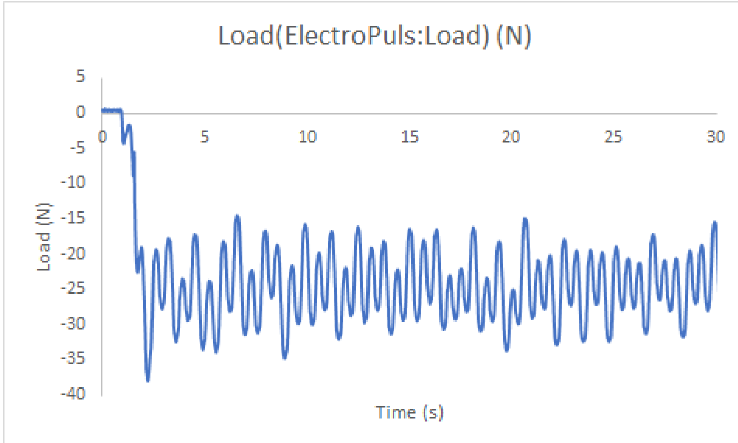


*Figure 31: Load (N) vs. Time (s) Output from Cooked Bone #2 at 3 Hz Frequency with 50 N of Force; test was done to establish if the frequency was suitable and if the force value could be achieved.*

### 6.1.2 Troubleshooting - Determining a Frequency

On March 11th, 2021 the second round of preliminary testing was conducted by the group. Various changes were made during this test. Small fresh bones were used instead of cooked bones during this round of testing. The cross-sectional area was calculated for each bone, and the strain was altered by one power of ten to reflect 300 microstrain. During the first round of testing, the data presented itself in an erratic, non-sinusoidal pattern. In an attempt to solve this, the frequency was set to 1 Hz rather than 2 or 3 Hz during this test. The input measurements corresponding to Small Fresh Bone #6 is shown in Table 11 below. Figure 32 below shows the output force values obtained during the first thirty seconds of the test.

*Table 9: Small Fresh Bone #6 Input Measurements (3/11/21)*

| Bone # | Modulus of Bone ($N/m^2$) | Strain | Cross Sectional Area ($m^2$) | Applied Force Necessary F=.003AE | Bone Length | Displacement (m) | Cycles | Frequency |
|---|---|---|---|---|---|---|---|---|
| Mini Bone 6 (Part 3) | 17000000000 | 0.0003 | $4.8645 * 10^{-5}$ | 50 | 0.0696 | N/A | 2100 | 1 Hz |

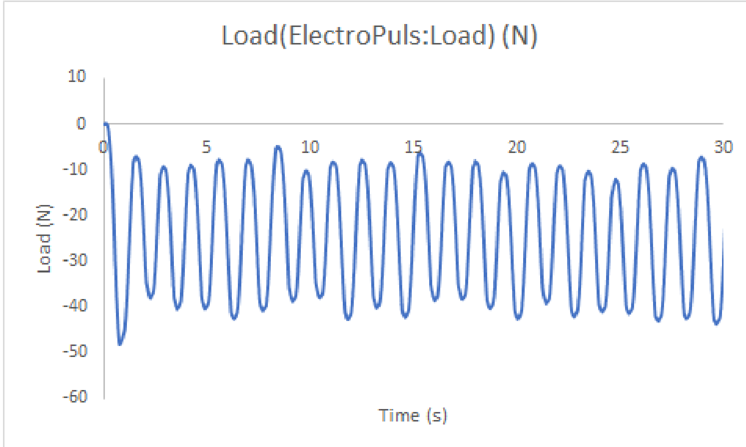


*Figure 32: Load (N) vs. Time (s) Output (Small Fresh Bone #6) at 1 Hz Frequency with Force of 50 N; test method frequency was adjusted to produce a more sinusoidal data pattern.*

### 6.1.3 Troubleshooting - Observing Displacement Increase Over Time

During the first thirty seconds on the test, the force value cycled between 0 and 50 N. This test produced a graph that behaved sinusoidally and reached desired force values. Instead of applying a calculated force value, this test was given a set 50 N end-of-cycle value to observe the cycling of the test. The test was set to include 3600 cycles, 1 cycle being one downward and one upward stroke. The test ran at a rate of 1 Hz (.5s downward stroke, .5s upward stroke). The test ran for around 700 cycles before it was stopped for observation. The team also was able to see that displacement increased over time, proving that fatigue was occurring. Because the Instron ElectroPuls works in reverse, the negative displacement values correlate to displacement accumulation on the specimen. Figure 33 below shows the displacement detected during the first 700 cycles conducted on Small Fresh Bone #6.

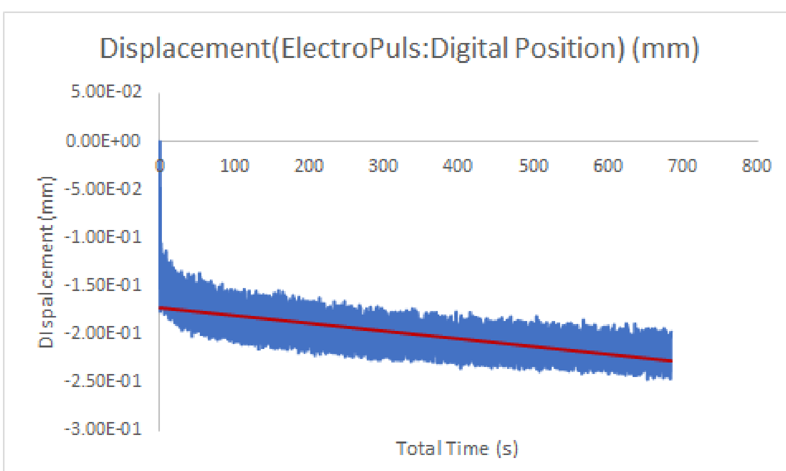

*Figure 33: Displacement (mm) vs. Time (s) at 1Hz Frequency with Force of 50 N (Small Fresh Bone #6); test established that displacement increases over time as the bone experiences damage accumulation.*

### 6.1.4 Troubleshooting - Force vs. Displacement Control

Another round of testing occurred on March 15th, 2021. After consideration of the obstacles the group experienced in the first three rounds of testing, additional changes were made in preparation for this round. This test was utilizing displacement control, rather than force control for observation purposes.The ideal displacement was determined using equations for strain using the original length of the bone and the desired strain, 300 microstrain. The test was set to include 5000 cycles (1 cycle=downward and upward stroke). The test ran at a rate of 3 Hz (.165s downward stroke, .165s upward stroke). The test ran for around 1500 cycles before it was stopped for observation. The input measurements for Small Fresh Bone #1 are shown in Table 13 below. The output force values during the first thirty seconds of the test on Small Fresh Bone #1 are shown in Figure 34 below. The cycling was less sinusoidal at this rate. The group observed that force decreased over time, proving that fatigue was occurring. The test was ended because the bone was no longer in contact with the fixturing at that point due to fatigue. The displacement values during this test were set to cycle between 0 and 0.02 mm. The displacement values achieved during this test are shown in Figure 35 below.

*Table 10: Small Fresh Bone #1 Input Measurements (3/15/21)*

| Bone # | Modulus of Bone (N/m$^2$) | Strain | Cross Sectional Area (m$^2$) | Applied Force Necessary F=.003AE | Bone Length | Displacement (m) | Cycles | Frequency |
|---|---|---|---|---|---|---|---|---|
| Mini Bone 1 | 17000000000 | 0.0003 | 4.7783 * 10$^{-5}$ | 243.69 | 0.06911 | 2.0733 * 10$^{-5}$ | 4350 | 3 Hz |

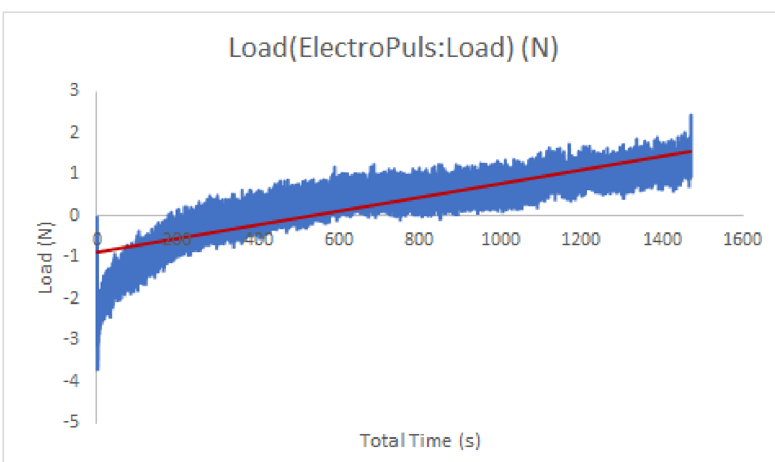


*Figure 34: Load (N) vs.Time (s)at 3 Hz Frequency (Small Fresh Bone #1); test allowed for observation of force decrease over time as displacement was controlled.*

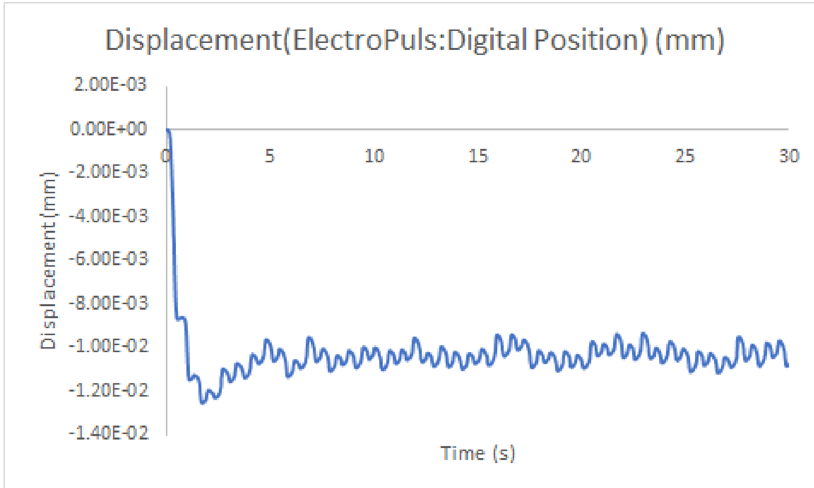


*Figure 35: Displacement (mm) vs. Time (s) at 3 Hz Frequency (Small Fresh Bone #1); further shows that 3 Hz frequency does not achieve the desired sinusoidal pattern.*

Although displacement control yielded valuable results, the team decided not to continue with this approach. Within the test, the bone experienced more damage and the force applied to the bone decreased over time. Eventually, the amount of force applied to the bone reached a zero value, as the cross-head of the Instron no longer came in contact with the bone. Due to this, the number of iterations within specimens would be inconsistent. The amount of data that could have been collected using displacement control proved to be less than with force control. Also, utilizing force control was decided to be more physiologically relevant to this project. In human motion, the amount of force applied during impact remains constant for each individual. Therefore, maintaining a constant force throughout a test sequence has a direct application to human motion.

### *6.2 Preliminary Testing Discussion*

After conducting four rounds of preliminary testing, we were able to collect valuable data and information during each stage. Overall, the group observed that a frequency value of 1 Hz provides the most sinusoidal data. Previous tests conducted at a frequency of 3 Hz were unable to reach the desired force values within the allotted time frame. The group also discovered that both the displacement control and force control methods produced expected results. During a displacement controlled analysis, the displacement force changes incrementally while the reaction depends on the stiffness of the material. The reaction force represents the force necessary to apply a particular displacement. In load controlled analysis, the load applied to the specimen changes incrementally while the displacement results depend on the stiffness of the structure. During the first round of preliminary testing, the group discovered that the M10 bolts being used to secure the bottom assembly were too long for the threaded holes in the table below the machine. Therefore, the bottom fixture could not be secured to the top of the face of the table. In order to combat this, shorter M10 bolts were ordered. The wing nuts attached to the fixture also resulted in an assembly problem. The wing nuts interfered with the top of the bolts, resulting in insecurity at all locations within the sliding slot portion of the assembly. In order to overcome this obstacle, wing nuts with a smaller turning radius were ordered.

## *6.3 Impacts of Final Design*

### 6.3.1 Economics

While our method and fixturing had an initial constraint to our budget of $1,250, the cost was much lower than that. We were able to be economical when developing fixturing that utilized the same fixturing for the axial and bend tests as well as minimizing the material needed for securing the bones. Though the cost of our method and fixturing is low, applying the project to a clinical setting raises the economic impact. Utilizing a CT scan is necessary for our bone prep to most accurately find the values needed before fatigue testing takes place. Additionally, for clients with bone stress injuries, this would be a more timely and possibly expensive process to go to when analyzing the biomechanics of their injury. We believe these methods could become more commonly used by professionals, doctors, athletic trainers, and physical therapists. It may be a procedural appointment and analysis covered by insurance if the efficiency is high enough in understanding, preventing and predicting these injuries.

### 6.3.2 Environmental and Sustainability

At this stage of the development, there are no significant environmental impacts. In this case, the environmental effects would be caused by the manufacturing of the fixturing. However, with a small scale and only need for one fabrication of these parts, there is no impact on the environment. The polyurethane plastic used in the resin potting is not enough to have a significant environmental concern.

### 6.3.3 Societal Impact

The methods are designed to understand damage accumulation in human metatarsals. In doing so, a runner or athlete can understand bone stress injuries. We developed a systematic way of understanding the fatigue loading with a user-chosen unique force value, frequency of cycles and orientation of the bone. Bone stress injuries could be predicted and prevented with our method that can account for the varying activities amongst athletes. If the use of the information gained from this testing became widespread amongst athletes that apply cyclic loading to their feet, mainly running and jumping athletes, the amount of bone stress injuries overall will decrease. It would help people with foot pain live a healthier and more pain free life.

#### 6.3.4 Political and Ethical Concerns

There are no applicable political ramifications or significant ethical impacts of our project. Currently, there are no mileage restrictions amongst NCAA athletes or professional athletes .If enough data was collected to understand damage accumulation in runners, there could be regulated target or maximum average mileage for injury prevention. An ethical concern would be the user must be well educated and versed with use of the fixtures and mechanical testing device and methods. It is important to be able to interpret and make conclusions about the data in its future use. The goal of the device is to understand bone stress injuries more, this knowledge would be used to help as many people as possible, regardless of their socioeconomic status.

#### 6.3.5 Health and Safety Impact

Our project will promote understanding of stress injuries within metatarsals, promoting healthier practice concerning bone health. In all, the project will decrease stress injuries due to overuse and fatigue in runners. While the sensor system will be used to understand damage accumulation and help predict these injuries, there are still a multitude of other causes and factors for bone stress injuries. An example being low mineral bone density. Safety issues are possible with the use of our testing fixtures and methods. The use of the Instron Electropuls 3000 is a dynamic and complicated testing machine. The extensive features and controls allow for physiologically relevant testing conditions but pose the risk of safety to be of higher concern. Before use of testing fixturing and methods, the user should attend a training of the devices.

# 7. Design Validation

---

## *7.1 Methodology Summary*

The team had to work through many trial and error periods to establish our final software method. After contemplating the idea of displacement control, where the load cell would extend a set distance and cause a varying force, it was ultimately decided that it was less physiologically relevant to human motion. Although the team initially planned to test a frequency of 3 Hz preliminary tests revealed that the lower the frequency, the more clear and sinusoidal the data output would be. Working through these two issues was crucial for finalizing the method, and the team ended up with a process that yielded very valuable results.

A sample size of 10 avian tibia was used. For each tibia, a unique force value was found. In order to find the unique force value, we utilized image processing programs. The first program used was Materialise Mimics, which allowed us to take the CT scan and have functional 3D models. By manipulating the orientation, we could capture the cross section of the midpoint of the bone. To reiterate from our previous research, the midpoint cross section would give us the point at which the stress would be highest in the bone. Once these images were determined and converted in a dicom file format, they were transferred to another program titled ImageJ. This program could take our midpoint cross section image and calculate area and pixel value statistics of user-defined selection. We used this data to determine the force we would be applying to each bone. It allowed us to be consistent in applying physiological relevant forces that replicate high strain activity. The cross sectional area of each tibia was found using ImageJ, as shown in Figure 36 below.

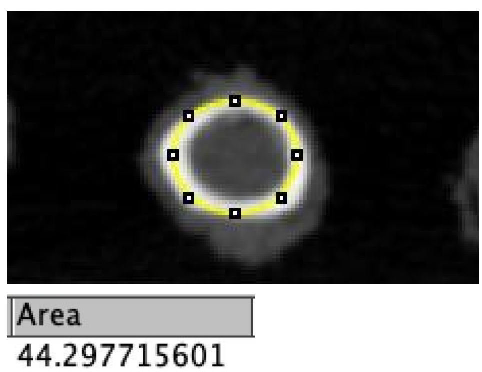


*Figure 36: Cross-sectional area in ImageJ of tibia midpoint*

Using the desired microstrain, 300 microstrain, and the standard modulus of bone, 17 GPa, a unique force value was found for each bone.

$$F = A_{cross-sectional} \times Elastic\ Modulus \times Microstrain$$

Once the methodology was established, the team completed final testing. These unique force values were inputted into the Bluehill software for incorporation into the test cycles. Since the Bluehill method was set to be in force control, the force to which the test will operate could be controlled. An individual test cycle involved the load cell of the Instron ElectroPuls extending vertically, compressing the tibia axially until the desired force was met, and returning back to a zero position within the frequency of 1 Hz for 30,000 cycles. The 1 Hz frequency was established due to the more sinusoidal nature of the force-displacement curve. With cleaner sinusoidal patterns, the group could better evaluate the data being collected by the Instron ElectroPuls. The test ran for 30,000 cycles, which when paired with the frequency of 1 Hz was completed within a 10-11 hour period. After each test was complete, the data from Bluehill was exported in Excel files. From these files, the data could be graphically analyzed in the manner that was found to be most appropriate. Shown below, in Figure 37, is an example of the Bluehill WaveMatrix screen as a test was being run. The two graphs on the bottom of the screen were important to monitor during testing, to ensure that the sinusoid and loads were consistent, and that we could see changes in the displacement over time.

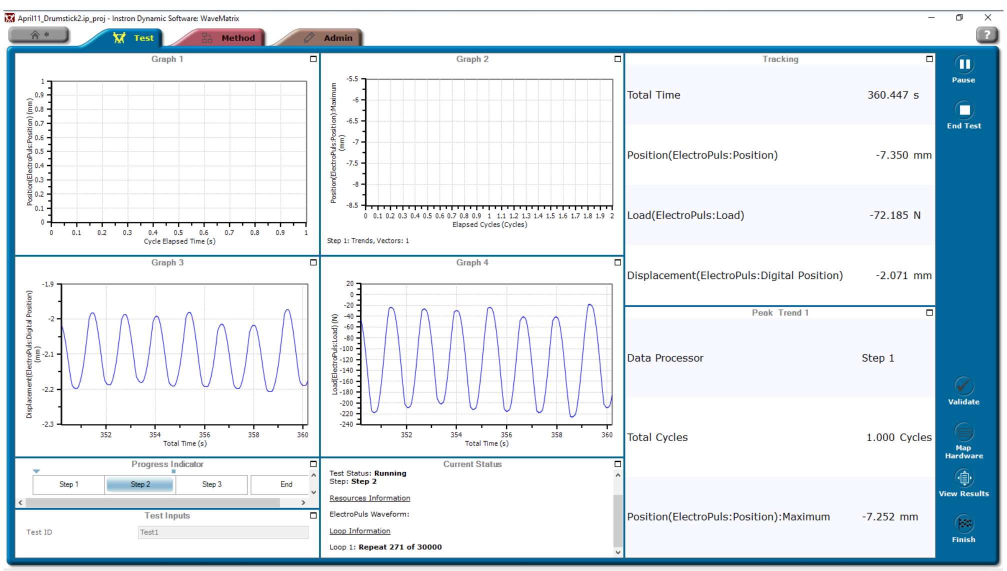


*Figure 37: Screen capture of Bluehill software as test was proceeding*

## *7.2 Summary of Data Collection*

Within the scope of this project, it was important to analyze how the displacement of the machine related to the number of cycles performed. The displacement experienced by the machine directly correlates to the displacement changes within the specimen. As displacement increases, damage accumulates within the bone. A complete graphical summary of the data set can be seen below in Table 14. Over the 30,000 cycles, a trend line was generated for displacement data. The slope of this trendline depicts the degree to which bone decay was generated over the testing interval, which can be seen on each of the graphs within the equation of the line. Within observing the accumulated data, knowledge can be drawn about when injury begins and how it progresses over time. Displacement during cyclic loading on each of the ten avian tibias is shown in Figures 38 through 47 below.

*Table 11: Data Collected from Testing 4/9/21 to 4/16/21*

| Bone # | Modulus of Bone (N/m$^2$) | Strain | Cross Sectional Area (m$^2$) | Applied Force Necessary F=.003AE | Bone Length | Displacement (m) | Cycles |
|---|---|---|---|---|---|---|---|
| 1 | 17000000000 | 0.0003 | 5.0014 * 10$^{-5}$ | 255.07 | 98.20e$^{-3}$ | 25000[1] | 1 |
| 2 | 17000000000 | 0.0003 | 4.8768 * 10$^{-5}$ | 248.72 | 97.92e$^{-3}$ | 30000 | 1 |
| 3 | 17000000000 | 0.0003 | 4.9889 * 10$^{-5}$ | 254.43 | 93.29e$^{-3}$ | 30000 | 1 |
| 4 | 17000000000 | 0.0003 | 4.8398 * 10$^{-5}$ | 246.83 | 93.04e$^{-3}$ | 30000 | 1 |
| 5 | 17000000000 | 0.0003 | 4.5843 * 10$^{-5}$ | 233.80 | 95.61e$^{-3}$ | 30000 | 1 |
| 6 | 17000000000 | 0.0003 | 5.0028 * 10$^{-5}$ | 256.16 | 95.10e$^{-3}$ | 30000 | 1 |
| 7 | 17000000000 | 0.0003 | 4.0001 * 10$^{-5}$ | 204.00 | 95.61e$^{-3}$ | 30000 | 1 |
| 8 | 17000000000 | 0.0003 | 4.3294 * 10$^{-5}$ | 220.80 | 94.86e$^{-3}$ | 30000 | 1 |
| 9 | 17000000000 | 0.0003 | 4.4297 * 10$^{-5}$ | 225.91 | 96.72e$^{-3}$ | 30000 | 1 |
| 10 | 17000000000 | 0.0003 | 3.9462 * 10$^{-5}$ | 201.25 | 96.20e$^{-3}$ | 20000[1] | 1 |

[1]Test was ended prior to the ideal 30,000 cycles. This was due to unforeseen interference with the computer controlling the software, and consequently the hardware.

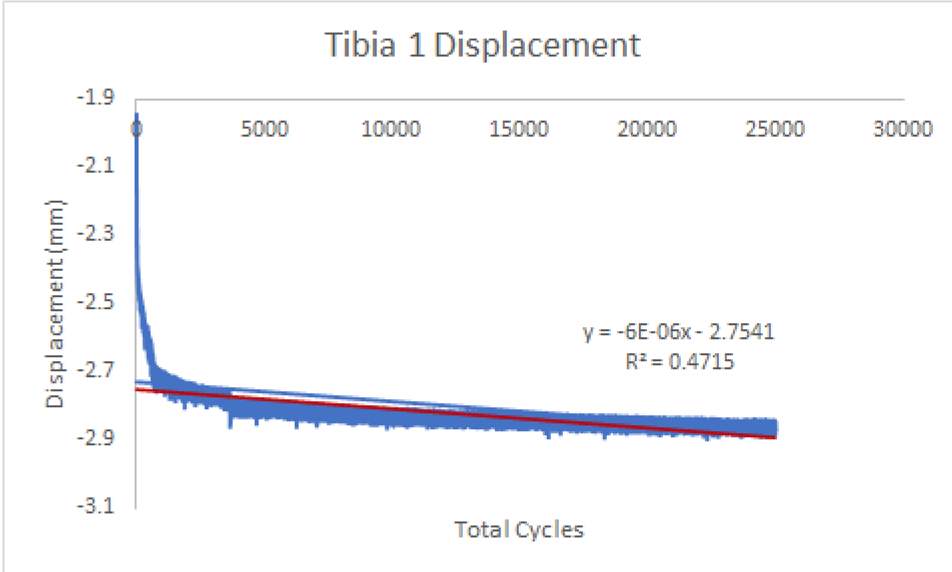


*Figure 38: Tibia 1 Displacement (mm) over 25,000 Cycles*

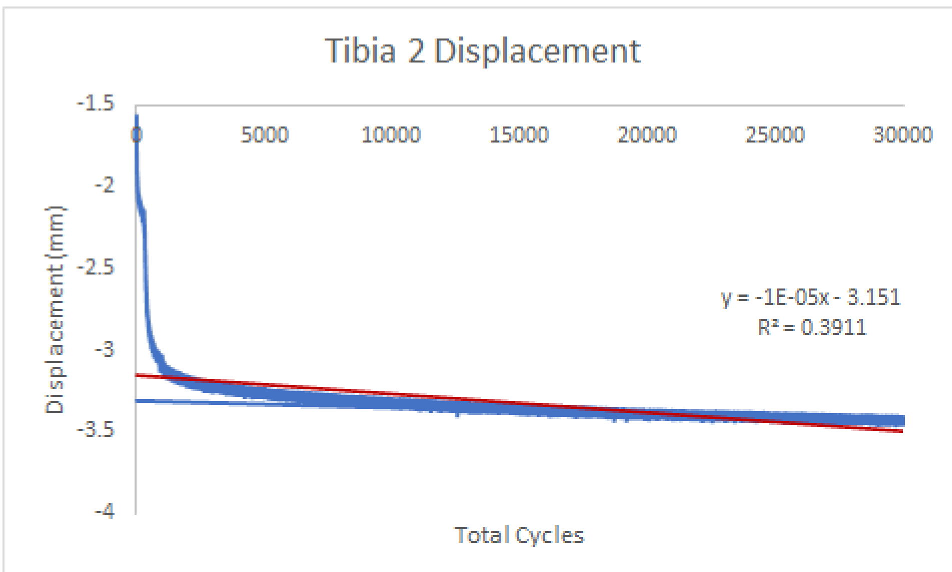


*Figure 39: Tibia 2 Displacement (mm) over 30,000 Cycles*

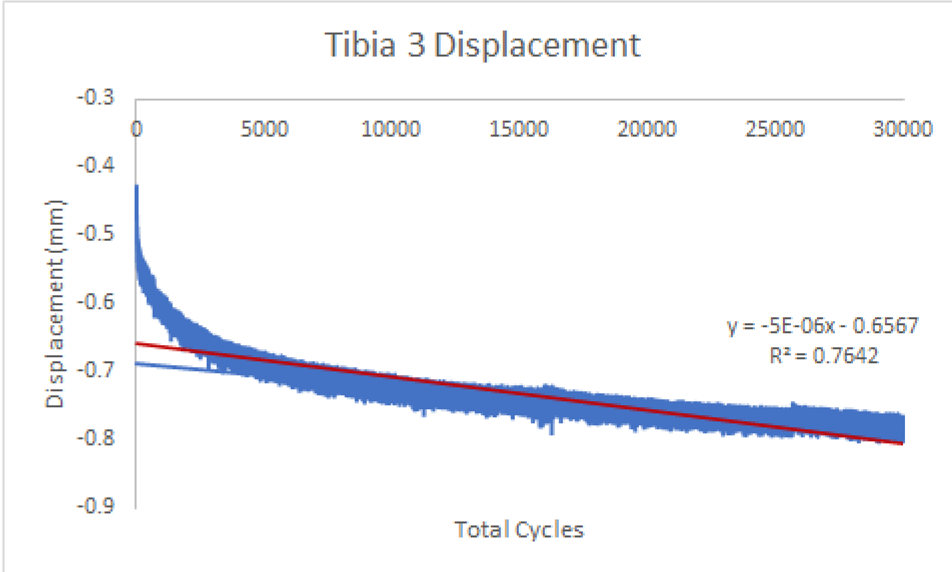


*Figure 40: Tibia 3 Displacement (mm) over 30,000 Cycles*

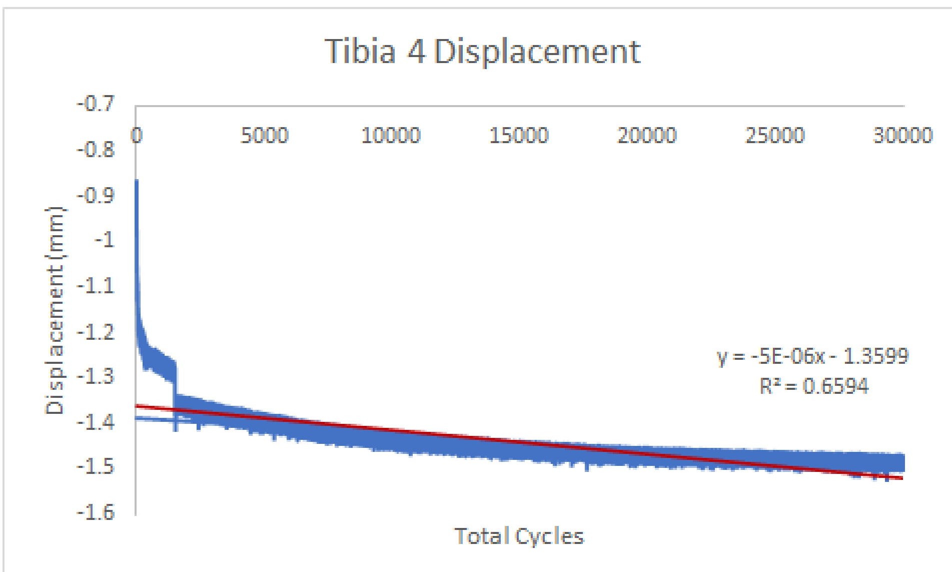


*Figure 41: Tibia 4 Displacement (mm) over 30,000 Cycles*

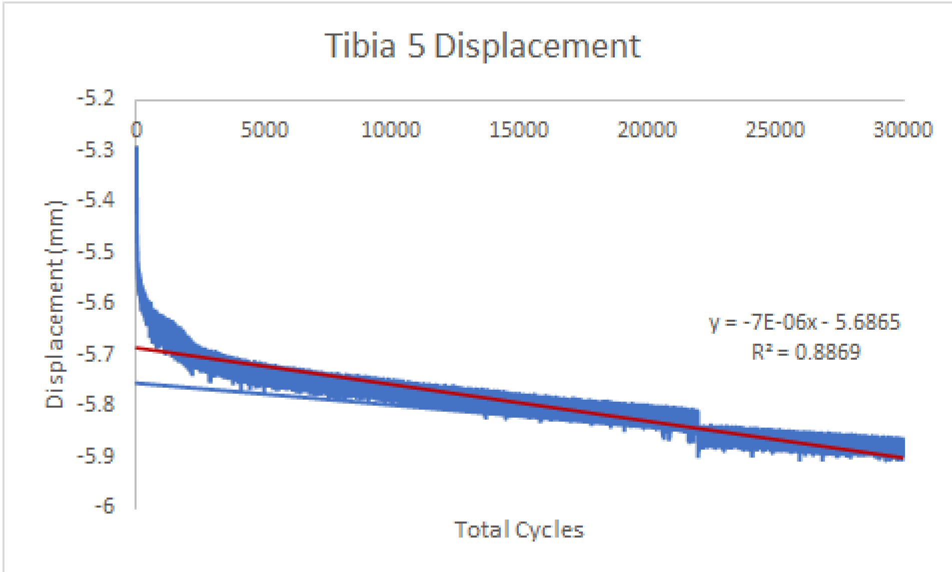


*Figure 42: Tibia 5 Displacement (mm) over 30,000 Cycles*

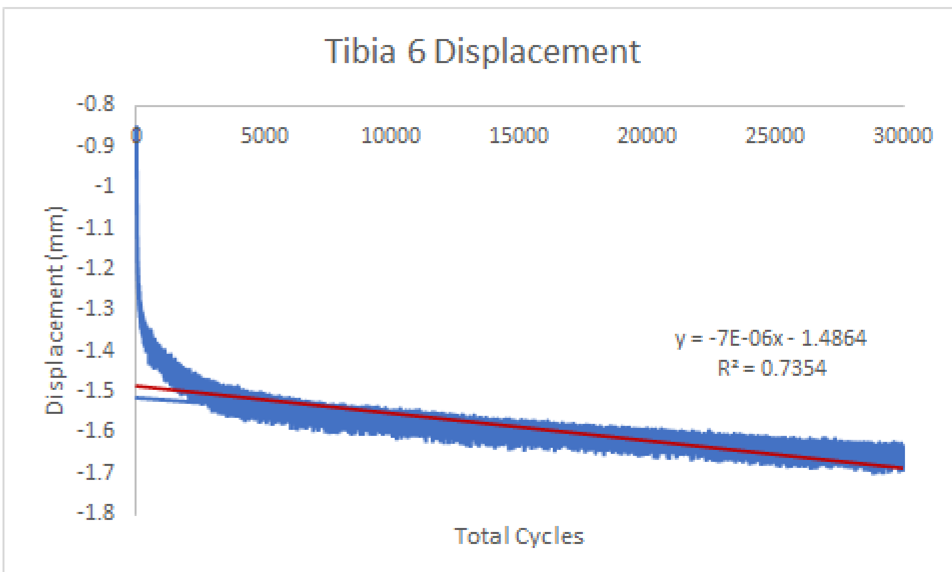


*Figure 43: Tibia 6 Displacement (mm) over 30,000 Cycles*

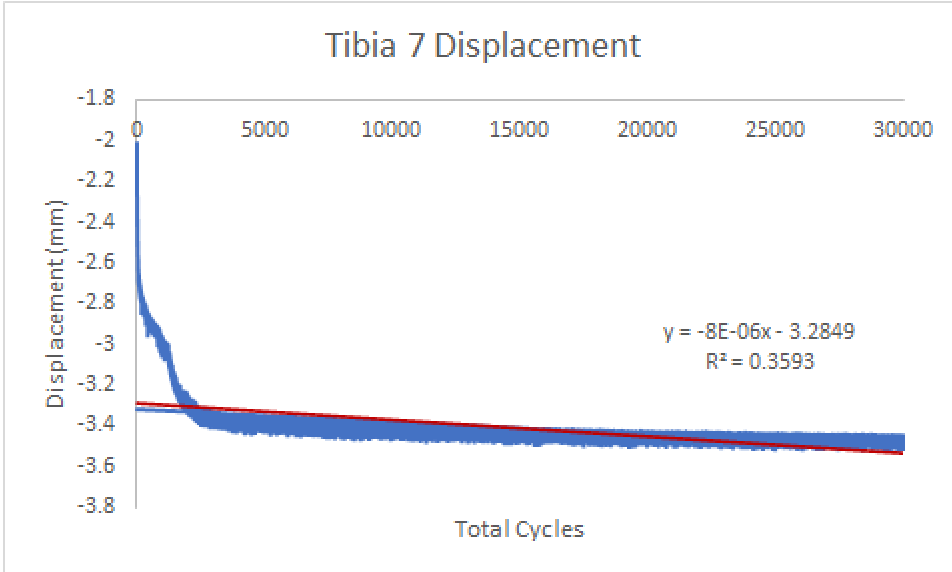


*Figure 44: Tibia 7 Displacement (mm) over 30,000 Cycles*

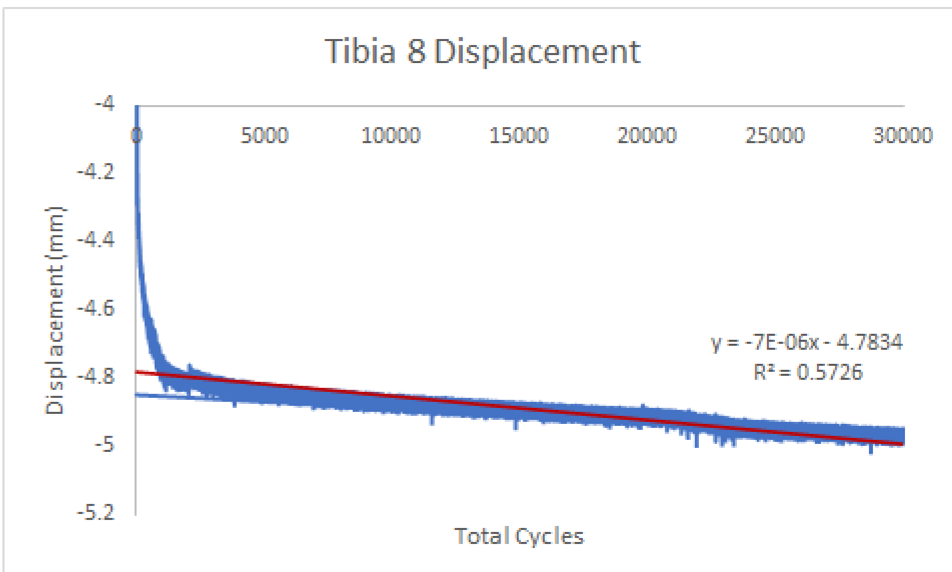


*Figure 45: Tibia 8 Displacement (mm) over 30,000 Cycles*

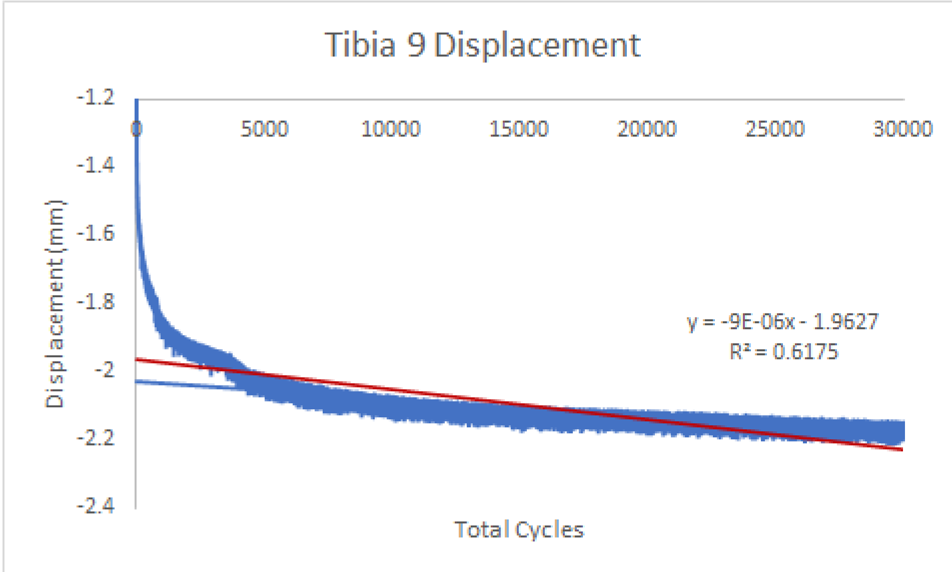


*Figure 46: Tibia 9 Displacement (mm) over 30,000 Cycles*

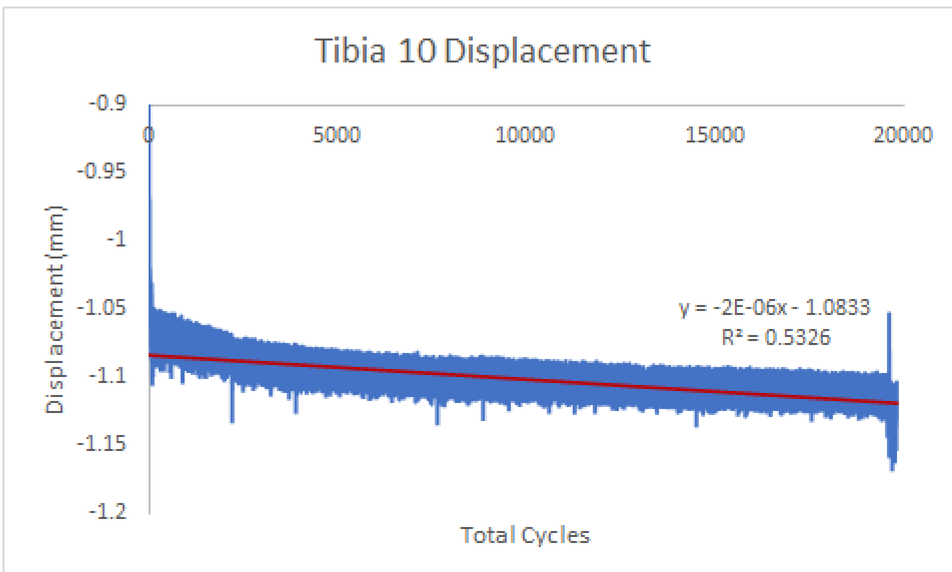


*Figure 47: Tibia 10 Displacement (mm) over 20,000 Cycles*

## *7.3 Data Collection Analysis and Results*

### 7.3.1 Standard Deviation and Average Calculations

As one can see from the graphs and table above, the bones experienced a drastic displacement shift within the first 1,000 cycles and then leveled off to steady damage accumulation throughout the remainder of the test sequence. The trendline depicts the rate at which damage accumulated over the 30,000 cycle period. Even though each tibia had differing unique force values, there was little deviation between the slope of the displacement trendlines. The mean displacement trendline slope value of the sample size was found to be $-6.6e^{-6}$

mm/cycle. The standard deviation between the slopes of displacement trendlines was found to be 2.154e$^{-6}$ mm/cycle. The curation of these results is a proof of concept that the fixturing and methodology designed within this project can produce valuable data for studies of fatigue damage. This data can be also used to predict damage accumulation over longer periods of time and be related to human metatarsal bone damage under similar loading conditions.

### 7.3.2 Stiffness Reduction Analysis

Using the raw data collected from the Bluehill WaveMatrix software, the original stiffness of the whole bone was determined using the following formula:

$$Stiffness_{Whole\ Bone} = F_{Applied\ by\ Instron} \times Displacement_{First\ Iteration}$$

Once the original stiffness was determined, stiffness values for 10%, 20%, and 50% stiffness reduction were calculated by multiplying the original stiffness by 0.9, 0.8, and 0.5, respectively. Following this, the displacement necessary to achieve 10%, 20%, and 50% stiffness reduction was calculated using the formula:

$$Displacement\ to\ Achieve\ \%\ Stiffness\ Reduction = F_{Applied\ by\ Instron} \div \%\ Stiffness\ Reduction$$

For 10% and 20% stiffness reduction, the displacement to achieve the % stiffness reduction could be manually located within the raw data outputted by Bluehill WaveMatrix. This displacement value was directly associated with a particular cycle number within the span of the testing sequence. This method was utilized since 10% and 20% stiffness reductions were experienced within 30,000 cycles by the most of the bones.

50% stiffness reduction was not experienced by any of the bones within the 30,000 cycles and for this reason, the amount of cycles to achieve a 50% stiffness reduction had to be estimated. To calculate this, the group set the displacement required to reach a 50% stiffness reduction equal to the trendline created from the displacement versus cycles graph and solved for the amount of cycles. The only bone that did not experience 10% and 20% stiffness reduction within the first 30,000 cycles was Bone 5. For this bone, the cycles to achieve each stiffness reduction benchmark were calculated using the method described for the 50% stiffness reduction. The spreadsheet containing the full set of calculations is linked in Appendix J. The table below shows the cycles to achieve 10%, 20%, and 50% stiffness reduction for each of the 10 specimens. Values highlighted in orange were found from raw Instron data and data highlighted in blue was calculated from the trendlines.

*Table 12: Cycles required to achieve 10%, 20%, and 50% stiffness reduction.*

| Cycles Required to Achieve 10% Stiffness Reduction | Cycles Required to Achieve 20% Stiffness Reduction | Cycles Required to Achieve 50% Stiffness Reduction |
|---:|---:|---:|
| 15 | 335 | 230263 |
| 7 | 65 | 11938 |
| 5 | 90 | 39486 |
| 7 | 45 | 84460 |
| 37095 | 143277 | 716658 |
| 7 | 20 | 37665 |
| 11 | 50 | 113783 |
| 5 | 10 | 166160 |
| 7 | 30 | 42952 |
| 10 | 70 | 322863 |

# 8. Concluding Thoughts

## *8.1 Future Recommendations*

Our team recommends that when this project is continued the testing includes bending force. This was in our team's original plan because bending force and axial force in combination replicate running biomechanics in the foot. Due to time restrictions we were unable to carry this portion of the testing out. We also recommend testing on human metatarsal bones rather than avian bones. Although avian bones are similar in modulus to human bones, actual testing on human metatarsals can give much more accurate data on the goal of our project, which is to better understand fatigue accumulation in the human foot. Further analysis is also recommended, including examination of crack propagation at each interval of reduced stiffness. This can give insight to further treatment and understanding, which would help to answer our research question. Lastly, an automated hydration system would make the process easier as it would lessen the time for team availability to manually hydrate the bone every few hours during testing. Figure 48, below, shows an example of an automated spray bottle our team designed, but did not get to use during testing.

*Figure 48: Automated Spray Bottle System using an Arduino Uno*

### *8.2 Conclusion*

The objectives of our project included designing a method and fixture to further understand and better treat athletes that have foot injuries from running. In the grand scheme of our project, our team successfully completed our goals of designing a working mechanical fixture and method to collect accurate data, represented in a sinusoidal wave. Overall, we had a strong design process that consisted of multiple iterations, test failures and successes. Our project was intended to be configurable for future testing of different kinds of bones, axial and bending testing, as well as achieving reproducible results. Based on our results and significance, we feel as though we accomplished this portion of configurability. Although we did not get a chance to complete all of our test runs and bending tests, we truly believe we have contributed greatly to the bigger picture of the project, to help better understand metatarsal injury and develop potential treatment.

# References


1. Pegrum, J., Crisp, T., & Padhiar, N. (2012). Diagnosis and management of bone stress injuries of the lower limb in athletes. *BMJ: British Medical Journal, 344*(7854), 35-40. Available at http://www.jstor.org/stable/41552000.

2. Dennis R. Carter, William E. Caler, Dan M. Spengler & Victor H. Frankel (1981) Fatigue Behavior of Adult Cortical Bone: The Influence of Mean Strain and Strain Range, Acta Orthopaedica Scandinavica, 52:5,481-490, DOI: 10.3109/17453678108992136

3. “Metatarsal Fractures,” *Physiopedia*. [Online]. Available: https://www.physio-pedia.com/Metatarsal_Fractures. [Accessed: 11-Oct-2020].

4. Stuart J. Warden, PT, PhD, FACSM1,2, Irene S. Davis, PT, PhD, FACSM, FAPTA, FASB3,4, , “Management and Prevention of Bone Stress Injuries in Long-Distance Runners,” *Journal of Orthopedic & Sports Physical Therapy*. [Online]. Available: https://www.jospt.org/doi/full/10.2519/jospt.2014.5334.

5. Sun, X., Yang, Y., Wang, L., Zhang, X., & Fu, W. (2018). Do Strike Patterns or Shoe Conditions have a Predominant Influence on Foot Loading?. *Journal of human kinetics*, *64*, 13–23. https://doi.org/10.1515/hukin-2017-0205

6. Wei, Z., Zhang, Z., Jiang, J., Zhang, Y., & Wang, L. (2019). Comparison of plantar loads among runners with different strike patterns. *Journal of sports sciences*, *37*(18), 2152–2158. https://doi.org/10.1080/02640414.2019.1623990

7. A. A. E. I. W. P. L. A; “Effects of fatigue and load variation on metatarsal deformation measured in vivo during barefoot walking,” *Journal of biomechanics*. [Online]. Available: https://pubmed.ncbi.nlm.nih.gov/11955501/. [Accessed: 11-Oct-2020].

8. Alexandra Abbott, Mackenzie L. Bird, Emily Wild, Symone M. Brown, Greg Stewart & Mary K. Mulcahey (2020) Part I: epidemiology and risk factors for stress fractures in female athletes, The Physician and Sportsmedicine, 48:1, 17-24

9. Ackerman KE, Cano Sokoloff N, DE Nardo Maffazioli G, Clarke HM, Lee H, Misra M. Fractures in Relation to Menstrual Status and Bone Parameters in Young Athletes. *Med Sci Sports Exerc*. 2015;47(8):1577-1586. doi:10.1249/MSS.0000000000000574

10. Rizzone KH, Ackerman KE, Roos KG, Dompier TP, Kerr ZY. The Epidemiology of Stress Fractures in Collegiate Student-Athletes, 2004-2005 Through 2013-2014 Academic Years. *J Athl Train*. 2017;52(10):966-975

11. Currey, John D.. *Bones : Structure and Mechanics*, Princeton University Press, 2006. ProQuest Ebook Central, http://ebookcentral.proquest.com/lib/wpi/detail.action?docID=1441378.

12. Hughes, Julie M et al. "The role of adaptive bone formation in the etiology of stress fracture." *Experimental biology and medicine (Maywood, N.J.)* vol. 242,9 (2017): 897-906. doi:10.1177/1535370216661646 https://www.ncbi.nlm.nih.gov/pmc/articles/PMC5407583/

13. Sun, X., Yang, Y., Wang, L., Zhang, X., & Fu, W. (2018). Do Strike Patterns or Shoe Conditions have a Predominant Influence on Foot Loading?. *Journal of human kinetics*, *64*, 13–23. https://doi.org/10.1515/hukin-2017-0205

14. Firminger, C., Fung, A., Loundagin, L., & Edwards, W. (2017). Effects of footwear and stride length on metatarsal strains and failure in running. *Clinical Biomechanics*, *49*, 8-15. doi: 10.1016/j.clinbiomech.2017.08.006

15. Fritton, S., J. McLeod, K., & Rubin, C. (2000). Quantifying the strain history of bone: spatial uniformity and self-similarity of low-magnitude strains. *Journal Of Biomechanics*, *33*(3), 317-325. doi: 10.1016/s0021-9290(99)00210-9

16. Petrisor, Brad & Ekrol, Ingri & court-Brown, Charles. (2006). The Epidemiology of Metatarsal Fractures. Foot & ankle international / American Orthopaedic Foot and Ankle Society [and] Swiss Foot and Ankle Society. 27. 172-4. 10.1177/107110070602700303.

17. Kawaguchi, A. (2018). Metatarsal Fracture. Retrieved from https://ota.org/for-patients/find-info-body-part/3723

18. Materialise mimics. (n.d.). Retrieved October 06, 2020, from https://www.materialise.com/en/medical/mimics-innovation-suite/mimics

19. Kourtis, L. (2008). VA-BATTS: Stresses in bone sections with inhomogeneous material properties. Retrieved January, 2021, from https://simtk.org/plugins/following/follow-info.php

# Appendix A: Glossary of Terms

---

Avian - relating to birds
Damage Accumulation - a process of cycle-by-cycle aggregation in a material undergoing fluctuating stresses and strains
Distal - away from the main mass or origins; in the appendages, the free end
Compression - the reduction in volume caused by an increase in pressure
Cancellous - having a porous structure made up of intersecting plates and bars that form small cavities or cells
Cortical- dense outer surface of bone that forms protective layer around internal cavity
Epidemiology- branch of medicine dealing with the incidence, distribution, and possible control of diseases and other factors relating to health
Fatigue- condition characterized by a lessened capacity for work and reduces efficiency of accomplishment
Hysteresis - phenomenon in which the value of a physical property lags behind changes in the effect causing it
Lateral- away from or relatively father from the median plane
Medial - toward or relatively near to the median plane
Microdamage- damage formed at the microscopic level of bone that occurs in response to skeletal loading
Periosteum- dense layer of vascular connective tissue enveloping the bones except at the surfaces of the joints
Plane- a surface, real or imaginary, along which any two points can be connected by a line
Propagation- the spreading or transmission of something
Remodeling- the process of undergoing structural reorganization, alteration, or renewal
Resin- a sticky, flammable, organic substance that is insoluble in water
S-N curve- a plot of the magnitude of an alternating stress versus the number of cycles to failure for a given material
Stiffness-resistance of the body to an external force that deforms its initial shape
Stress- failure of bone to adapt to a new load, causing an imbalance in bone remodeling
Stress Fracture- a fracture of bone caused by repeated mechanical stress
Tension- the condition of being stretched

# Appendix B: Important Equations

$\sigma total = \sigma c + \sigma b$

where, $\sigma c$ = compressive stress
$\sigma b$= bending stress

$\sigma c = \frac{F}{A}$

where, F = force
A = cross-sectional area

$\sigma b= \frac{My}{I}$ where, My = a=Moment
I = inertia = second moment of area

$\varepsilon= \frac{L-Lo}{Lo} = \frac{\Delta L}{Lo}$

where, ε= strain
L = length
Lo = original length

$\sigma = E * \varepsilon$

where, σ = Stress
E = elastic modulus (assume linear elastic)
ε= strain

$F = \sigma * A$

where, F = target force
A = cross-sectional area

$k = \frac{F}{\Delta d}$

where, F = force
$\Delta d$ = displacement

$\sigma m = \frac{\sigma max + \sigma min}{2}$

where, $\sigma m$= mean stress
$\sigma max$ = maximum stress
$\sigma min$ = minimum stress

$bx = \frac{L}{2}$ where, $bx$= bone midpoint (maximum moment)

L = bone length

# Appendix C: VA Batts Download

---

“VA-BATTS: Stresses in bone sections with inhomogeneous material properties”: A software tool to calculate bending, axial, torsional, and transverse shear stresses within bone cross sections having inhomogeneous material properties

Note:
After unzipping you should have two folders, totaling ~19MB: 1) Data; 2) Program

# Appendix D: VA Batts Code "main.m"

---

```
%% 0. INPUT

% Flexural Loads
        Mx          = 0;            %in N.m
Mx=Mx*1000;
My          = 0;            %in N.mm
% OR (3pt bending)
Qx      = 0;    %in N
Qy      = 0;    %in N
z_pos       = 1;    %in mm
% Axial Loads
P       = 0;    %in N
        T       = 1;
T=T*1000;
% Torsion displacement


%DONT forget to edit image2density.m to match your image to density calibration relation. See manual for
examples

%% Model parameters
nodes_r  = 16;          % number of nodes in the radial direction
nodes_th = 64;          % number of nodes along the circumference

zone_width=11;          %select search zone width for boundary search refinement


%%
nodes_th = 4*round(nodes_th /4); %Adjust number of nodes along circumference
                        %so that it is divided by 4 (for meshing
                        %purposes)
%% 1. Import the image.
[A, resolution, slice_z, filename]=read_section_image;
if A==0;break;end
A=double(A); A_original=A;
plot_image(A, 1, ['Subject: ' filename '  Slice Position: ' num2str(slice_z) '  - Original Scan [original units]'], [1,2]);
%Interactively select bone by cropping the original image.
max_A_value = max(max(A));
A = max_A_value*imcrop(A/max_A_value);
A_original = A;
plot_image(A, 1, ['Subject: ' filename '  Slice Position: ' num2str(slice_z) '  - Original Scan [original units]'], [1,2]);
bar_handle=colorbar;

%% 2. perform image processing to "clean" image
% A is the original image in image units
% A_bin is the logical map used to mask the image.
```

```
plot_image(A_original, 1, ['Subject: ' filename '  Slice Position: ' num2str(slice_z) '  - Original Scan [original units]'],
[1,2]);
bar_handle=colorbar;
canal_flag = determine_mesh_type;
temp_center = [size(A)/2];
limit = find_threshold_limits(A_original, canal_flag, 50);
segmentation_threshold=mean(limit);
[A, A_bin]  =   threshold_image(A_original, segmentation_threshold); %threshold image. segmentation_threshold is
the level in HUplot_image(A, 2, 'Cropped and Thresholded Image - [image units]', [2,2]); hold on
set(bar_handle,'YColor','w','FontSize',8,'Box','off','YLim',[limit(1), limit(2)]);
%% 3. Threshold image interactively and Calculate center of xsection
%Repeat thresholding and cropping.(left clicking)
%By selecting a point on the colorbar, it automatically uses it as
%a new threshold level and reiterates.
%By selecting a point on the image, it recalculates the center, and
%re-crops the image. Then the countour is found.
%Right clicking to confirm, exit this loop and proceed
but=1;
while (but==1)
figure(1); [selected_point(1),selected_point(2),but]=ginput(1);
        if but==1

        if selected_point(1)<1;
        segmentation_threshold=selected_point(2);
        else
        temp_center=selected_point;
        end
        [A, A_bin, ext_blob, int_blob] = interactive_threshold (A, A_original, temp_center,
segmentation_threshold, canal_flag);
        center_A            = find_center (A);            %find center of image

        plot_image(A, 2, 'Cropped and Thresholded Image - [image units]', [2,2]); hold on
        figure(2);plot(center_A(1),center_A(2),'r+');
        % 3A. Find the internal & external nodes
        [node_ext_polar, node_ext_cart, node_int_polar, node_int_cart] = detect_boundary (center_A, nodes_th,
canal_flag, ext_blob, int_blob);
        % Plot countour(s)
        ex_contour_handle=line(node_ext_cart(1:end-1,1), node_ext_cart(1:end-1,2), 'Marker','.',
'MarkerSize',8,'LineStyle','-','ButtonDownFcn','pickandmove(ex_contour_handle,[])');
        if canal_flag==1  %plot inner contour iff intramedulary canal is present
        in_contour_handle=line(node_int_cart(1:end-1,1), node_int_cart(1:end-1,2), 'Marker','.',
'MarkerSize',8,'LineStyle','-','ButtonDownFcn','pickandmove(in_contour_handle,[])');
        end
        drawnow
% 3B. Refine the boundary detection by creating a trust region around the
%previously detected boundary (zone), and then apply image partial voluming
%correction algorithms. Then re-detect boundary.
        [x_dimension, y_dimension ] = find_bounding_box(node_ext_cart, resolution);


 %define the width of the search zone based on whether there is thick enough
 %cortical bone on the periosteal surface. For distal/proximal bone,
```

```
 %cortical bone is thin, for midshaft cortical bone is thick therefore
 %search zone width can be wider
            if canal_flag==false
            zone_width = 7;
            end
            set(ex_contour_handle,'XData',node_ext_cart(1:end-1,1),'YData',node_ext_cart(1:end-1,2),
'Color','r','LineStyle','-','ButtonDownFcn','pickandmove(ex_contour_handle,[])');
            drawnow;

            [node_ext_polar] = refine_boundary(node_ext_polar,  A, center_A, zone_width,ex_contour_handle);

            node_ext_cart = polar2cart(node_ext_polar,center_A);
            set(ex_contour_handle,'XData',node_ext_cart(1:end-1,1),'YData',node_ext_cart(1:end-1,2),
'LineStyle','-','ButtonDownFcn','pickandmove(ex_contour_handle,[])');
            drawnow

            end % end if mouse click is left button : right click selected exit
end % end while loop

%Read back the vertex positions and Dismiss the events for the contour plots
node_ext_cart = [ get(ex_contour_handle,'XData'); get(ex_contour_handle,'YData') ]' ;
node_ext_cart = [node_ext_cart ; node_ext_cart(1,:)];
if canal_flag==1
            set(in_contour_handle,'ButtonDownFcn','')
            node_int_cart = [ get(in_contour_handle,'XData'); get(in_contour_handle,'YData') ]' ;
            node_int_cart = [node_int_cart ; node_int_cart(1,:)];
end

%% 4. Convert to cartesian coords and Mesh cross section.
%Convert seed node positions from cartesian to polar coordinates
  [node_ext_polar] = cart2polar (node_ext_cart, center_A);
%  node_ext_polar(:,1)=pi/2-node_ext_polar(:,1);       %the pi/2-  is there cause matlab is treating x,y in an inverse
way
  if canal_flag==1
  [node_int_polar] = cart2polar (node_int_cart, center_A);
%   node_int_polar(:,1)=pi/2-node_int_polar(:,1);       %the pi/2-  is there cause matlab is treating x,y in an inverse
way
  end
%

%% Create the mesh based on the external and internal nodes
[node_polar, element] = create_mesh(node_ext_polar(1:end-1,:), node_int_polar(1:end-1,:), nodes_r, canal_flag,
center_A);
% Convert to cartesian coordinates
node = polar2cart (node_polar, center_A);

% Calculate bounding box for bone. This can be compared to direct caliper
% measurements or x-ray images in order to determine segmentation accuracy
[x_dimension, y_dimension ] = find_bounding_box(node_ext_cart, resolution)
OD_mean = mean(node_ext_polar(:,2));

%% 5. Convert to material properties and find centers.
```

```
% A_d is the density image
% A_YM is the Young's Modulus image
% A_v is the Poisson's ratio image
center_A_bin       = find_center (A_bin);
[A_d]              = image2density(A,A_bin);          %convert HU to apparent density [gr/cm3]
[A_YM, A_G, A_v]          = density2elastic_props(A_d);        %convert apparent density [g/cm3] to YM [MPa]
G[MPa]
% Calculate center for each image
center_d           = find_center (A_d);
center_YM          = find_center (A_YM);
center_G           = find_center (A_G);

 total_BM = sum(sum(A_d));
BMD = total_BM/(x_dimension*2.3); % calculate BMD by taking the sum of mineral and divide by the total area of
the slice

%% 6. Convert nodes to real units: mm and assign material properties to each element.
% Then, determine the cross sectional properties
node_real(:,1)=node(:,1)*resolution(1); %[node_real] are the coordinates in real units (mm)
node_real(:,2)=node(:,2)*resolution(2); %[node]        are the coordinates in image units (pixels)
node_ext_cart(:,1)=node_ext_cart(:,1)*resolution(1);
node_ext_cart(:,2)=node_ext_cart(:,2)*resolution(2);
 if canal_flag==1
 node_int_cart(:,1)=node_int_cart(:,1)*resolution(1);
 node_int_cart(:,2)=node_int_cart(:,2)*resolution(2);
 end
% This will give the YM, G in Pa and centroid,area (in square mm) for each element
[YM, v, G, rho, area, centroid, center_mesh, center_mesh_E] = assign_material (node, node_real, element, A_YM,
A_G, A_v, A_d, resolution, nodes_th);
% %  For Benchmarking only
% %  YM=2*(1+0.33)*ones(length(YM),1);
% %      v=0.33*ones(length(v),1);
% %      G=1*ones(length(G),1);
% Plotting
figure(2); p_mesh=patch('Vertices', node, 'Faces', element,'FaceAlpha',0.3,'EdgeColor',[0.3 0.3 0.3]);
 set(p_mesh,'FaceVertexCData',repmat(YM,1,3)./max(YM), 'FaceColor', 'flat','FaceAlpha',1); drawnow;
 colormap gray; bar_handle=colorbar; set(bar_handle,'YColor','w','FontSize',8,'Box','off'); drawnow

%% 6. Calculate the sectional properties.
[I, J, I_principal, V,   I_E, J_E, I_E_principal, V_E,   I_G, J_G, I_G_principal, V_G] = section_properties (YM, G,
rho, centroid, area, center_mesh, center_mesh_E);
equivalent_diameter = 2*sqrt(sum(area)/pi);
%Set 0,0 at the middle
 node_real = node_real - repmat(center_mesh_E,length(node_real),1);
 centroid  = centroid  - repmat(center_mesh_E,length(element),  1);

                          node_ext_cart=node_ext_cart-repmat(center_mesh_E,length(node_ext_cart),1);
 if canal_flag==1; node_int_cart=node_int_cart-repmat(center_mesh_E,length(node_ext_cart),1); end
%% 7. Solve Shear problem
for bb=1:2
        if bb==1
        theta=1;
```

```
            else
            theta=T/K_mod
            end

[shear_stress, resultant_shear_stress, K_mod] = solve_FE_problem (node_real,element, YM, G, v, I_E, Qx, Qy,
theta);
torque = theta*K_mod
resultant_shear_stress_e = sqrt(shear_stress(:,1).^2+shear_stress(:,2).^2);
%resultant_shear_stress_e = resultant_shear_stress_e./((rho./1.92).^1.333);
resultant_shear_stress = elemental2nodal (resultant_shear_stress_e, node, element);
plot_contour(node_real , element, node_ext_cart,node_int_cart, resultant_shear_stress, 4, 'Shear Stresses' , [1 1],
'tau')
end
%quiver(centroid(:,1),centroid(:,2),shear_stress(:,1),shear_stress(:,2),0.65,'k'); drawnow
%% 8. Bending Stresses: use Beam theory to calculate bending stresses
[bending_stress_e] = calculate_bending (Mx, My, Qx, Qy, z_pos, P, I_E, node_real, area,centroid, YM,  [0 0]);
%bending_stress = bending_stress./((rho./1.92).^2);
[bending_stress] = elemental2nodal (bending_stress_e, node, element);
plot_contour(node_real, element, node_ext_cart, node_int_cart, bending_stress , 3, 'Out-of-Plane Normal Stresses' ,
[2 1], 'sigma'); drawnow
sigma_yield = 68 * rho.^2;
tau_yield   = 21.6 * rho.^1.65;
%Equivalent Stress (Tsai - Wu)
equivalent_stress = ( abs(bending_stress_e) ./ sigma_yield).^2 + (resultant_shear_stress_e ./ tau_yield).^2;
plot_contour(node_real, element, node_ext_cart, node_int_cart, equivalent_stress , 5, 'Equivalent Stress (Elliptical
Criterion)' , [1 2], 'sigma'); drawnow
yield=find(equivalent_stress>1);
yield_area = sum(area(yield)) / sum(area);

yield_plot = ones(length(equivalent_stress),3);
yield_plot(yield,1) = 0.8; yield_plot(yield,2)=0.2; yield_plot(yield,3)=0.2;
plot_image(A, 6, 'Failed Elements (red)', [2,2]); hold on
            figure(2);plot(center_A(1),center_A(2),'r+');
 p_mesh=patch('Vertices', node, 'Faces', element,'FaceAlpha',0.3,'EdgeColor',[0.3 0.3 0.3],'EdgeColor','None');
  set(p_mesh,'FaceVertexCData',yield_plot, 'FaceColor', 'flat','FaceAlpha',1); drawnow;
  bar_handle=colorbar; set(bar_handle,'YColor','w','FontSize',8,'Box','off'); drawnow


break


%% 9. Trace cortical and trabecular bone
trabecular = find(YM<8000);
cortical   = find(YM>8000);
marrow  = find(YM<2);
YM_plot = ones(length(YM),3);
YM_plot(trabecular,1) = 1; YM_plot(trabecular,2)=0.0; YM_plot(trabecular,3)=0.0;
YM_plot(cortical,2) = 1; YM_plot(cortical,1)=0.0; YM_plot(cortical,1)=0.0;
YM_plot(marrow,3) = 0; YM_plot(marrow,1)=0; YM_plot(marrow,2)=0;
plot_image(A, 7, 'Trabecular and Cortical Bone', [2,2]); hold on
            figure(2);plot(center_A(1),center_A(2),'r+');
p_mesh=patch('Vertices', node, 'Faces', element,'FaceAlpha',0.3,'EdgeColor',[0.3 0.3 0.3]);
```

```
 set(p_mesh,'FaceVertexCData',YM_plot, 'FaceColor', 'flat','FaceAlpha',1); drawnow;
 bar_handle=colorbar; set(bar_handle,'YColor','w','FontSize',8,'Box','off'); drawnow


trabecular_area = sum(YM_plot(:,1).*area);
cortical_area = sum(YM_plot(:,2).*area);
total_area =cortical_area+ trabecular_area
cortical_ratio = cortical_area/total_area
trabecular_ratio = 1-cortical_ratio


%% 10. ABAQUS export
extrusion_depth=100; extrusion_nodes=20; inhomogeneity=1;
abaqus_export2(node_real, element, YM, G, v, nodes_th, extrusion_depth, extrusion_nodes, 'test1.inp',
inhomogeneity)
```

# Appendix E: Mimics Scan Configurations

| | Midpoint | Value (/pixel) | File # | File name (mimics) | File name (dicom) |
|---|---|---|---|---|---|
| Bone #1.1 | 49.1 | 52.152 | 212 | "BSI_MQP_resliced_bone1.1" | "BSI_MQP_Dicom1.1_0212.dcm" |
| Bone #2.1 | 48.96 | 49.446 | 201 | "BSI_MQP_resliced_bone2.1" | "BSI_MQP_Dicom2.1_0201.dcm" |
| Bone #3.1 | 46.645 | 50.676 | 206 | "BSI_MQP_resliced_bone3.1" | "BSI_MQP_Dicom3.1_0206.dcm" |
| Bone #4.1 | 46.52 | 50.676 | 206 | "BSI_MQP_resliced_bone4.1" | "BSI_MQP_Dicom4.1_0206.dcm" |
| Bone #5.1 | 47.805 | 53.136 | 216 | "BSI_MQP_resliced_bone5.1" | "BSI_MQP_Dicom5.1_0216.dcm" |
| Bone #1.2 | ~47.55 | 48.216 | 196 | "BSI_MQP_resliced_bone1.2" | "BSI_MQP_Dicom1.2_0196.dcm" |
| Bone #2.2 | 48.54 | 50.184 | 204 | "BSI_MQP_resliced_bone2.2" | "BSI_MQP_Dicom2.2_0204.dcm" |
| Bone #3.2 | 47.43 | 51.66 | 210 | "BSI_MQP_resliced_bone3.2" | "BSI_MQP_Dicom3.2_0210.dcm" |
| Bone #4.2 | 48.36 | 49.2 | 200 | "BSI_MQP_resliced_bone4.2" | "BSI_MQP_Dicom4.2_0200.dcm" |
| Bone #5.2 | 48.1 | 49.2 | 200 | "BSI_MQP_resliced_bone5.2" | "BSI_MQP_Dicom5.2_0200.dcm" |
| Mini Bone #1 | 34.555 | 31.98 | 130 | "BSI_MQP_resliced_minibone1" | "BSI_MQP_minibone1_0130.dcm" |
| Mini Bone #2 | 35.715 | 37.146 | 151 | "BSI_MQP_resliced_minibone2" | "BSI_MQP_minibone2_0151.dcm" |
| Mini Bone #5 | 33.615 | 37.884 | 154 | "BSI_MQP_resliced_minibone3" | "BSI_MQP_minibone3_0154.dcm" |
| Mini Bone #4 | 36.055 | 36.408 | 148 | "BSI_MQP_resliced_minibone4" | "BSI_MQP_minibone4_0148.dcm" |
| Mini Bone #3 | 32.985 | 36.9 | 150 | "BSI_MQP_resliced_minibone5" | "BSI_MQP_minibone5_0150.dcm" |
| Mini Bone #6 | 34.805 | 39.852 | 162 | "BSI_MQP_resliced_minibone6" | "BSI_MQP_minibone6_0162.dcm" |
| Mini Bone #7 | 35.38 | 37.884 | 154 | "BSI_MQP_resliced_minibone7" | "BSI_MQP_minibone7_0154.dcm" |
| Mini Bone #8 | 36.23 | 42.066 | 171 | "BSI_MQP_resliced_minibone8" | "BSI_MQP_minibone8_0171.dcm" |
| Mini Bone #9 | 35.935 | 37.392 | 152 | "BSI_MQP_resliced_minibone9" | "BSI_MQP_minibone9_0152.dcm" |
| Mini Bone #10 | 37.6 | 38.13 | 155 | "BSI_MQP_resliced_minibone10" | "BSI_MQP_minibone10_0155.dcm" |

# Appendix F: Expense Report

| Name | Part Number | Quantity | Price | Ordered From |
|---|---|---|---|---|
| 316 Stainless Steel Wing Nut | 94543A420 | 1 | $4.48 | McMaster Carr |
| 18-8 Stainless Steel Hex Head Screw | 91287A347 | 1 | $11.35 | McMaster Carr |
| Structural Adhesive | 7605A11 | 1 | $6.50 | McMaster Carr |
| 18-8 Stainless Steel Socket Head Screw | 91292A218 | 1 | $10.94 | McMaster Carr |
| Multipurpose 6061 Aluminum - 4" Diameter (Length: 3 in) | 1610T37 | 1 | $25.93 | McMaster Carr |
| Multipurpose 6061 Aluminum - 2" Thick x 5" Wide (Length: 1/2 ft) | 8975K631 | 1 | $44.89 | McMaster Carr |
| Passivated 18-8 Stainless Steel Phillips Flat Head Screw - M3 x 0.5 mm Thread, 10 mm Long | 92010A120 | 1 | $4.89 | McMaster Carr |
| Rotary Shaft - 303 Stainless Steel, 1/4" Diameter, 9" Long | 1257K118 | 1 | $8.05 | McMaster Carr |
| 18-8 Stainless Steel Hex Head Screw - M6 x 1 mm Thread, 80 mm Long, Fully Threaded | 91287A354 | 1 | $7.52 | McMaster Carr |
| 18-8 Stainless Steel Socket Head Screw -M10 x 1.5 mm Thread, 35 mm Long | 91292A161 | 1 | $9.54 | McMaster Carr |
| 18-8 Stainless Steel Socket Head Screw -M10 x 1.5 mm Thread, 20 mm Long | 91292A157 | 1 | $6.46 | McMaster Carr |
| Multipurpose 6061 Aluminum - 1-1/2" Thick x 3" Wide (Length: 1/2 ft) | 8975K255 | 1 | $27.84 | McMaster Carr |
| 32 GB Flash Drive | - | 1 | $9.27 | Amazon |

## Appendix J: Link to Full Calculations Sheet

---

Data Analysis